Article

Cell

The DEAD-Box Protein Dhh1p Couples mRNA Decay and Translation by Monitoring Codon Optimality

Graphical Abstract

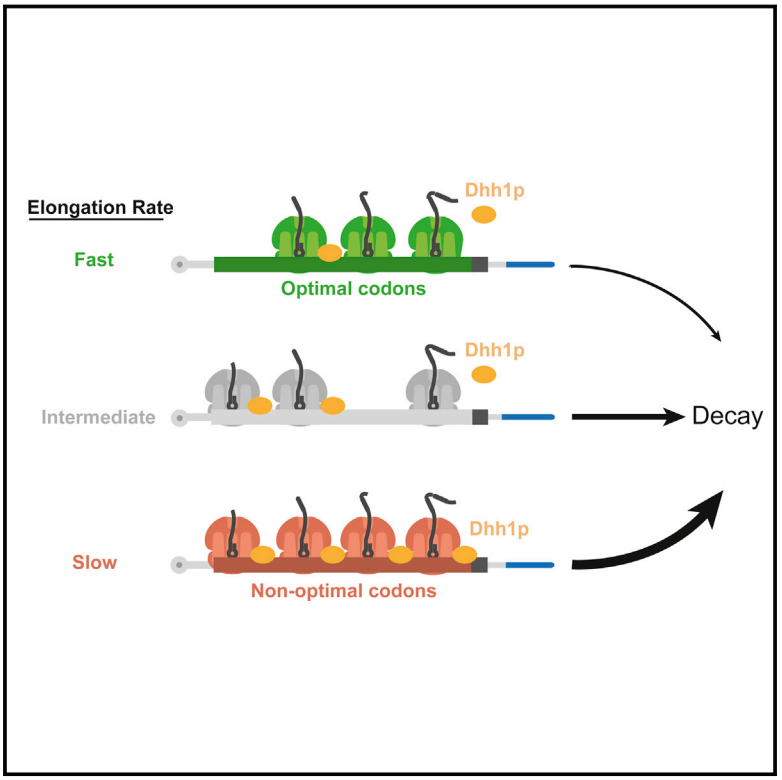

Authors

Aditya Radhakrishnan, Ying-Hsin Chen, Sophie Martin, Najwa Alhusaini, Rachel Green, Jeff Coller

Correspondence

ragreen@jhmi.edu (R.G.), jmc71@case.edu (J.C.)

In Brief

mRNA stability depends on codon optimality through a direct link to elongating ribosomes.

Highlights

- The codon-dependent rate of translational elongation impacts mRNA stability
- The DEAD-box protein Dhh1p associates with the translating mRNP
- Dhh1p couples translation to mRNA decay by sensing codon optimality

Data Resources

GSE81269
GSE46142

Radhakrishnan et al., 2016, Cell *167*, 122–132
September 22, 2016
http://dx.doi.org/10.1016/j.cell.2016.08.053

CellPress

Cell

Article

The DEAD-Box Protein Dhh1p Couples mRNA Decay and Translation by Monitoring Codon Optimality

Aditya Radhakrishnan,[1,2,4] Ying-Hsin Chen,[3,4] Sophie Martin,[3,4] Najwa Alhusaini,[3] Rachel Green,[2,*] and Jeff Coller[3,5,*]
[1]Program in Molecular Biophysics, Johns Hopkins University School of Medicine, Baltimore, MD 21205, USA
[2]Department of Molecular Biology and Genetics, Howard Hughes Medical Institute, Johns Hopkins School of Medicine, Baltimore, MD 21205, USA
[3]Center for RNA Molecular Biology, Case Western Reserve University, Cleveland, OH 44106, USA
[4]Co-first author
[5]Lead Contact
*Correspondence: ragreen@jhmi.edu (R.G.), jmc71@case.edu (J.C.)
http://dx.doi.org/10.1016/j.cell.2016.08.053

SUMMARY

A major determinant of mRNA half-life is the codon-dependent rate of translational elongation. How the processes of translational elongation and mRNA decay communicate is unclear. Here, we establish that the DEAD-box protein Dhh1p is a sensor of codon optimality that targets an mRNA for decay. First, we find mRNAs whose translation elongation rate is slowed by inclusion of non-optimal codons are specifically degraded in a Dhh1p-dependent manner. Biochemical experiments show Dhh1p is preferentially associated with mRNAs with suboptimal codon choice. We find these effects on mRNA decay are sensitive to the number of slow-moving ribosomes on an mRNA. Moreover, we find Dhh1p overexpression leads to the accumulation of ribosomes specifically on mRNAs (and even codons) of low codon optimality. Lastly, Dhh1p physically interacts with ribosomes in vivo. Together, these data argue that Dhh1p is a sensor for ribosome speed, targeting an mRNA for repression and subsequent decay.

INTRODUCTION

mRNA degradation represents a critical step in the regulation of gene expression. In budding yeast, most mRNAs are degraded by initial removal of the 3′ polyadenosine tail (Hsu and Stevens, 1993). This leads to subsequent cleavage of the 5′ cap structure in a process termed "decapping," followed by digestion of the mRNA body by a 5′ to 3′ exoribonuclease enzyme (Muhlrad et al., 1994). While the major pathway and the enzymes catalyzing mRNA turnover have been identified (Anderson and Parker, 1998; Hsu and Stevens, 1993; Muhlrad et al., 1994; Shoemaker and Green, 2012), a mechanism to account for disparate mRNA half-lives has been elusive. Recently, we discovered that codon optimality is a major feature that contributes to determining mRNA stability (Presnyak et al., 2015). Using a genome-wide RNA decay analysis, we found that stable mRNAs are enriched in optimal codons, whereas unstable mRNAs are enriched in non-optimal codons (Presnyak et al., 2015). These results establish the existence of coupling between active translation by ribosomes of an mRNA and its stability (Hu et al., 2009; Pelechano et al., 2015). Reporter studies recapitulated these striking genome-wide results (Presnyak et al., 2015). Similar effects of codon usage on mRNA stability were recently documented in bacteria and metazoans (Boël et al., 2016; Mishima and Tomari, 2016).

The idea that codon choice influences gene expression has long been understood (Dix and Thompson, 1989; Thomas et al., 1988). The inherent degeneracy of the genetic code leads to the possibility that synonymous codons are recognized distinctly by the ribosome as a function of subtle differences in tRNA availability, demand, and decoding fidelity and mRNA secondary structure propensity. All of these factors can lead to variability in codon-specific rates of translation (Drummond and Wilke, 2008; Gingold and Pilpel, 2011; Ikemura and Ozeki, 1983; Pechmann and Frydman, 2013). Codon optimality is a term coined to discuss the non-uniform recognition of each of the 61 codons by the ribosome based on supply and demand arguments (Pechmann and Frydman, 2013). Codon bias, which is the frequency at which distinct synonymous codons are present within the genome, is, in part, shaped by codon optimality (Novoa and Ribas de Pouplana, 2012). Codons that are evolutionarily enriched in highly translated mRNA transcripts are often optimal codons (i.e., triplets that are decoded by tRNAs of relatively higher abundance), whereas codons that exhibit no such selective bias are typically non-optimal and are decoded by tRNAs of relatively lower abundance. Since codon bias is distinct for every genome and represents a balance between selection, mutation, and genetic drift, codon optimality is often found to be distinct between species (Bulmer et al., 1991; Hershberg and Petrov, 2008; Man and Pilpel, 2007; Rocha, 2004). In broad terms, it is generally accepted that the speed at which the ribosome decodes is affected by the subtle distinctions in tRNA concentrations between synonymous sets of codons (Dong et al., 1996; Sørensen et al., 1989; Tuller et al., 2010; Varenne et al., 1984). Thus, tRNA abundance is a critical regulator of ribosome elongation rates and therefore can impact the efficiency of protein folding, protein stability, protein activity, and the coordinate expression of functionally related genes (Kim et al., 2015;

Pechmann and Frydman, 2013; Sander et al., 2014; Spencer et al., 2012; Yu et al., 2015; Zhang et al., 2009).

Attempts to observe differences in elongation rate that are dependent on codon identity and optimality using ribosome profiling (Ingolia et al., 2009), however, have been challenging. While a number of studies have found a modest correlation between codon optimality and ribosome occupancy (Charneski and Hurst, 2013; Ingolia et al., 2011; Li et al., 2012; Pop et al., 2014), others have observed increased ribosome occupancy on codons with low-abundance cognate tRNAs (Dana and Tuller, 2014; Gardin et al., 2014). There has been great effort to resolve these discrepancies, with recent work showing that coupling between codon optimality and ribosome occupancy can be masked by pretreatment of cells with translational inhibitors (Hussmann et al., 2015; Weinberg et al., 2016).

The regulation of elongation rate and post-translational events (i.e., protein folding and protein activity) by codon optimality is simply a consequence of functional tRNA concentration—a "passive response." On the contrary, the regulation of mRNA turnover by codon optimality likely represents a more active process, with the ribosome's elongation rate under constant surveillance by component(s) of the mRNA turnover complex. Herein, we focus on identifying a cellular factor that senses slow ribosomes to coordinate and couple translation and mRNA decay.

Dhh1p (DDX6) is a highly conserved and abundant DEAD-box protein previously implicated in translational repression (Carroll et al., 2011; Coller and Parker, 2005) and mRNA decay (Coller et al., 2001; Fischer and Weis, 2002; Presnyak and Coller, 2013). In budding yeast, loss of *DHH1* activity results in a block in mRNA decapping, but unlike other decapping regulators, this function is dependent on the translational status of the mRNA (Coller et al., 2001; Coller and Parker 2005). Moreover, previous studies showed that direct tethering of Dhh1p to the 3′ UTR of a reporter mRNA resulted in loss of protein production but dramatic ribosome accumulation on the message. These data suggest that Dhh1p directly impacts ribosome movement or processivity (Sweet et al., 2012).

Here, we demonstrate that Dhh1p is a critical factor in distinguishing between mRNAs containing optimal and non-optimal codons and targeting them for decay. mRNA-binding studies show that Dhh1p is more efficiently recruited by non-optimally coded mRNAs. In addition, ribosome occupancy is specifically modulated on optimally and non-optimally coded genes (and codons) by Dhh1p. Finally, Dhh1p binds to ribosomes in vivo. Together, these results suggest that Dhh1p is a sensor of slow ribosomes and communicates this information to the mRNA decay machinery to consolidate downstream output.

RESULTS

Codon Optimality Is a Powerful Determinant of mRNA Decay

We have previously demonstrated that codon optimality is a major determinant of mRNA degradation in *Saccharomyces cerevisiae*. In our previous work, we established a biological metric that indicates the overall contribution of each of the 61 codons toward mRNA stability. We referred to this metric as the codon stabilization coefficient (CSC). Because these CSC scores correlated nicely with previously established metrics for optimality (Pechmann and Frydman, 2013; dos Reis et al., 2004), we argued that mRNA stability is influenced by translational elongation rate.

An analogous metric is the tRNA adaptation index (TAI), which quantifies the relative cellular "supply" of cognate and near-cognate tRNAs for a given codon (dos Reis et al., 2004). However, in this study, we use a slightly different metric referred to as the species-specific TAI (sTAI) (Sabi and Tuller, 2014). While these quantities are largely identical on a per-codon basis, the parameters for sTAI are derived purely through sequence information, whereas the original definition of TAI takes into account actual gene expression data. As we here characterize codon effects on gene expression and translation, we opted for the more naive metric (sTAI) to avoid the potential pitfall of data overfitting.

Here, we began our study by following up on earlier results (Presnyak et al., 2015) and creating 11 constructs that differ slightly in codon optimality, as defined by both CSC and sTAI. Importantly, all 11 constructs produce the identical polypeptide (i.e., the His3 protein; Figure 1A) but do so using a distinct mixture of synonymous optimal or non-optimal codons. Between these constructs, the percentage of optimal to non-optimal codons varies by only 10%, allowing for coverage of the complete range of optimal codon content seen within the genome (Figure 1A). The assignment of codons within each construct was done randomly using a computer algorithm (Figure S1A; Table S1), where the average CSC and sTAI for each construct were found to be highly correlated (Figure S1B). We monitored the mRNA decay rate using a temperature-sensitive allele of RNA polymerase II (i.e., *rpb1-1*). Transcription was inhibited by quickly shifting cells from a permissive temperature to a restrictive temperature (from 24°C to 37°C). Time points following this shift were taken, and mRNA was analyzed by northern blot. As shown in Figure 1B (left), the mRNA half-life varies with changing optimal codon content. These data agree with our previous findings that codon optimality is a major determinant of mRNA stability (Presnyak et al., 2015).

Importantly, protein synthesis rates are sensitive to stresses such as temperature shifts. Thus, the use of the temperature-sensitive allele *rpb1-1* to monitor mRNA degradation has the potential to be misleading. To address this issue, we used an independent approach to test the influence of codon optimality on mRNA decay. For this experiment, we placed the same 11 constructs in Figure 1B (left) under the control of the inducible *GAL1* promoter. Cells were grown in galactose at 24°C to mid-log phase. Transcription was then inhibited by adding glucose but maintaining the cells at 24°C. Following the addition of glucose, time points were taken, and mRNA was analyzed by northern blot. Here, we also observed that codon optimality has a powerful influence on mRNA decay (Figure 1B, right). In fact, the mRNA half-lives observed using the *GAL1* shutoff approach are nearly identical to those obtained using an *rpb1-1* shutoff (Figure 1C). In both experiments, we observe the complete range of observed decay rates (from 3 min to 45 min) simply by changing codon composition without altering the polypeptide sequence. Together, these results indicate that codon optimality is a major

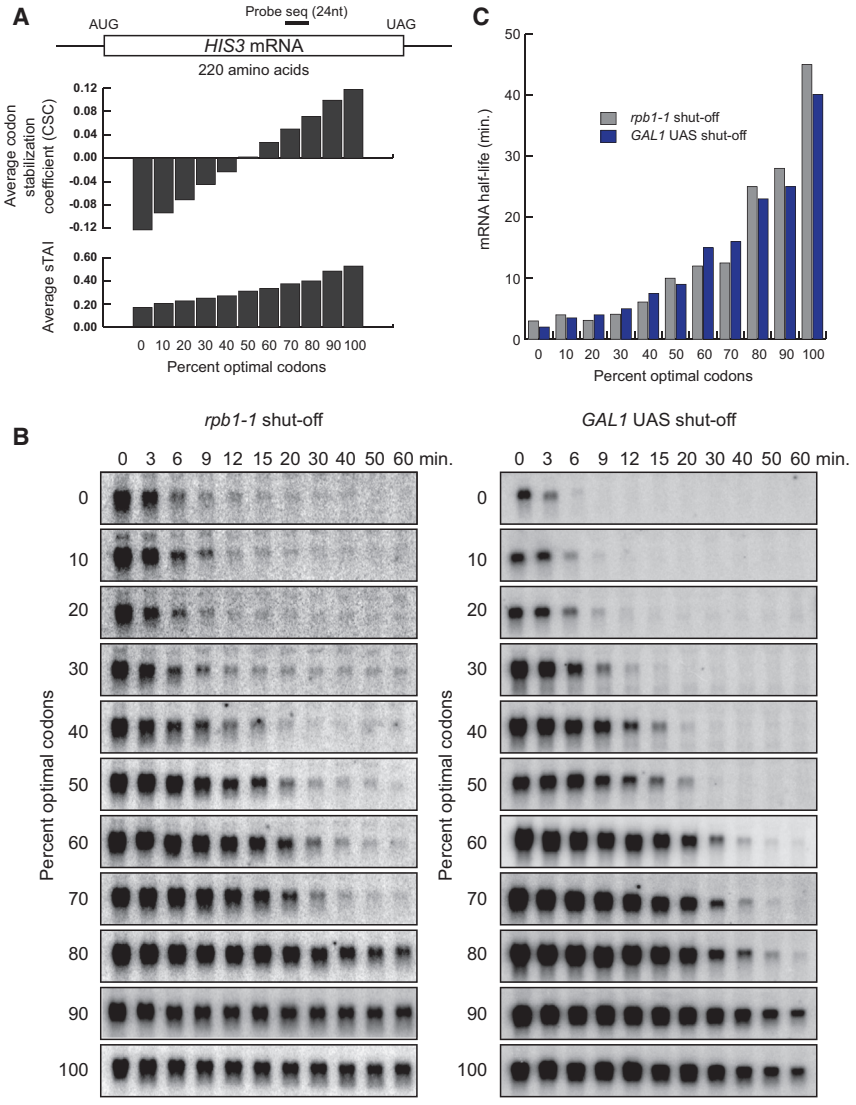

Figure 1. Codon Optimality Is a Powerful Determinant of mRNA Stability

(A) Representation of the *HIS3* mRNA reporter. Each reporter encodes the exact same polypeptide sequence but is composed of different codon composition of varying optimality. The average codon stabilization coefficient (CSC) and species-specific tRNA adaptation index (sTAI) for each construct are shown.

(B) Northern blots of the *HIS3* reporter series following transcriptional shutoff in a *rpb1-1* strain (left). The right panel shows the same reporters re-cloned with the *GAL1* inducible promoter. Shown are northern blots following transcriptional inhibition with glucose.

(C) Graphs of the half-lives of the mRNA reporters in (B).

See also Figure S1 and Table S1.

contributor to mRNA stability. Importantly, even 10% changes in codon content have powerful effects on mRNA stability.

Dhh1p Stimulates the Degradation of mRNAs of Low Codon Optimality

As a known regulator of mRNA decapping and a translational repressor, two qualities that seem potentially relevant to the direct coupling between mRNA decay with codon optimality, we asked whether Dhh1p is a critical factor in mediating this connection by determining the influence of Dhh1p on the decay of RNA reporters of differing codon optimalities. For this, we utilized two reporter constructs (Figure 2A) that encode the same polypeptide but are composed of either all optimal codons (OPT) or synonymous non-optimal (NON-OPT) codons (Presnyak et al., 2015). The reporter mRNAs were expressed under the control of the *GAL1* upstream activating sequence (UAS), allowing us to monitor mRNA decay as described above. As shown in Figure 2B, the OPT mRNA (sTAI = 0.539) is more stable than the NON-OPT mRNA (sTAI = 0.167) in wild-type (WT) cells ($t_{1/2}$ = 17 min versus 3 min, respectively), consistent with our previous findings (Presnyak et al., 2015). Importantly, however, in the absence of *DHH1*, the OPT mRNA's half-life is unchanged relative to WT, while the NON-OPT is substantially stabilized (Figure 2B). Indeed, in the absence of *DHH1*, the stability of the NON-OPT mRNA now mirrors that of the OPT mRNA. As a control, we repeated these experiments in cells lacking *PAT1* (another regulator of mRNA decapping), *CCR4* (the major deadenylase), or *DCP2* (the catalytic subunit of the decapping enzyme). In each case, the stability of both the OPT and NON-OPT mRNA increases, as anticipated for proteins with known roles in mRNA decay, but the difference in stability of the OPT and NON-OPT constructs persists. Together, these data demonstrate that Dhh1p is a critical factor in determining the influence of codon optimality on mRNA decay.

We next measured the influence of Dhh1p on the decay of the 11 reporters used in Figure 1B. The reporter mRNAs were expressed in *dhh1Δ* cells under the control of the *GAL1* UAS, allowing us to determine mRNA half-life by glucose-dependent transcriptional inhibition. RNA levels were quantitated by northern blot. As shown in Figure 2C, we observed that loss of *DHH1* had the most dramatic effect on the mRNA reporters of low codon optimality (Figure 2C; 0%–50% optimal codons). The reporters bearing a high percentage of optimal codons were predominately unaffected by loss of *DHH1*. The data are consistent with our hypothesis that Dhh1p controls mRNA degradation by sensing translational elongation rate.

We extended our reporter analysis of Dhh1p to the entire genome by performing mRNA sequencing (mRNA-seq) in WT versus *dhh1Δ* cells (Figure 2D). Binning mRNAs by sTAI, we find that low sTAI mRNAs are preferentially stabilized in the

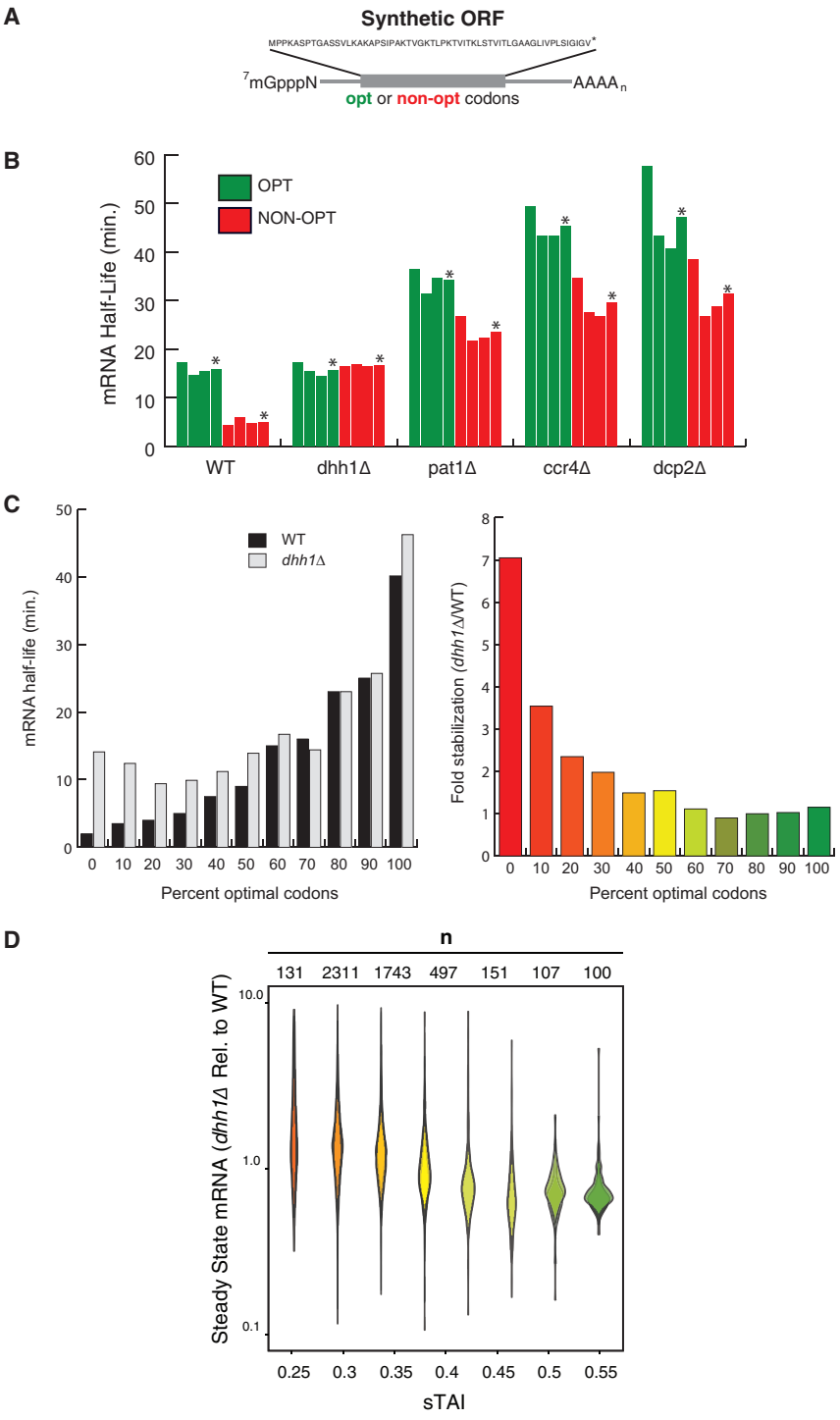

Figure 2. Dhh1p Selectively Stimulates the Decay of mRNAs with Low Codon Optimality

(A) Representation of the synthetic mRNAs (SYN) and the encoded polypeptide sequence. Optimal (OPT) or non-optimal (NON-OPT) codons encoding the same peptide were used. The artificial peptide has no similarity to any known proteins.

(B) The half-lives of SYN OPT and NON-OPT mRNAs in WT and different mutant strains were obtained from *GAL1* shutoff experiments. Quantitations were normalized to the amount of *SCR1* RNA. *Denotes average of three experiments.

(C) Half-lives of *HIS3* reporters from Figure 1B (*GAL1* UAS constructs) in WT or *dhh1Δ* cells. Right panel indicates fold stabilization in a *dhh1Δ* cells versus WT.

(D) Quantification of steady-state levels of mRNAs transcripts by RNA sequencing (RNA-seq) in *dhh1Δ* cells (reads per kb per million [RPKM]) relative to WT cells (RPKM). mRNA transcripts are binned by sTAI, a numerical proxy for overall optimality. Shown are two biological replicates. A two-tailed Mann-Whitney test shows that low-optimality mRNAs (sTAI = 0.25, median [Med.] = 1.52) are enriched relative to high optimality mRNAs (sTAI = 0.55, Med. = 0.72) upon Dhh1p depletion ($U = 1668$, $p < 2.2 \times 10^{-16}$). See also Figure S2.

absence of *DHH1*. To address possible concerns that sTAI is not directly reporting on the effects of codons on translation but is serving as a proxy for GC content and/or mRNA structure, we looked at the correlation between sTAI and GC content (Figure S2A) and asked whether the differential steady-state levels of mRNA transcripts in WT cells versus *dhh1Δ* exhibited a dependence on the GC content of the transcript. They do not (Figure S2B). Thus, the major trend that emerges as significant from our analysis of the *dhh1Δ* strain relative to the WT is a correlation between sTAI and mRNA levels. Furthermore, our method for binning is a consequence of natural codon usage, i.e., most genes within the genome are relatively non optimal with a subset that are predominantly optimal. We attempted to address concerns that the observed phenotype could be entirely due to the effect of a few outlier genes with extreme values of sTAI. Thus, we performed this analysis using equivalent bin sizes rather than bins equivalently distributed across the ordinate of sTAI (Figure S2C), where, ultimately, a similar trend emerges.

mRNA levels under constitutive overexpression of Dhh1p via a glyceraldehyde-3-phosphate dehydrogenase (GPD) promoter, however, show no such trends with respect to optimality, suggesting that availability of downstream components (decay factors) may be limiting in these cells (Figures S2D and S2E). Indeed, endogenous Dhh1p concentrations within the cell are already in large excess relative to other decapping factors (Ghaemmaghami et al., 2003). While the genome-wide data represent a steady-state analysis of mRNA levels, which necessarily misses some of the texture of a kinetic analysis, the data are nevertheless strikingly consistent with the kinetic observations made with reporter mRNAs.

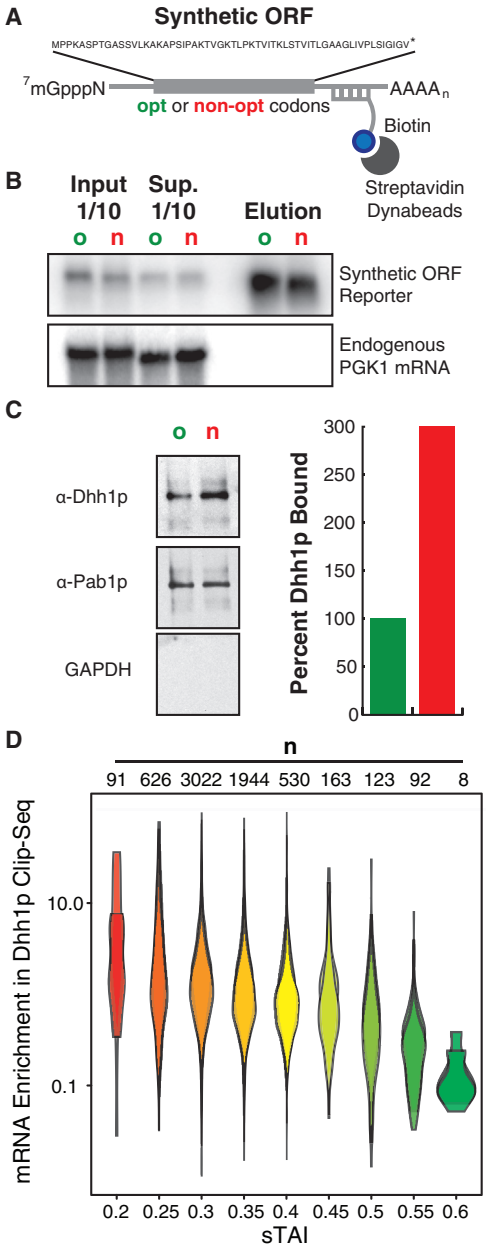

Figure 3. Dhh1p Preferentially Binds to mRNAs with Low Codon Optimality

(A) Representation of the reporters and experimental design used for mRNA pull-down. A tag sequence was inserted in the 3′ UTR of the SYN reporters for pull-down.

(B) Northern blot for the SYN mRNAs pull-downs. *PGK1* mRNA was probed as a control of specificity. o, optimal; n, non-optimal.

(C) Western blot showing the amount of Dhh1p, Pab1p, and GAPDH pulled down by the SYN mRNAs. Quantitations of Dhh1p were normalized to mRNA levels from eluates in (B).

(D) Reanalysis of previously performed CLIP sequencing (CLIP-seq) on Dhh1p calculating enrichment of transcripts bound to Dhh1p relative to WT conditions, where transcripts are binned by sTAI. Shown are two biological replicates. A two-tailed Mann-Whitney test shows that low-optimality mRNAs (sTAI = 0.25, Med. = 2.02) are preferentially bound to Dhh1p relative to high-optimality mRNAs (sTAI = 0.55, Med. = 0.32) ($U = 304$, $p = 7.1 \times 10^{-9}$).

Dhh1p Binds Preferentially to mRNA of Low Codon Optimality

The Dhh1p-dependent selective degradation of mRNAs of low sTAI predicts that Dhh1p will preferentially associate with these messenger ribonucleoproteins (mRNPs). To test this, we determined the relative amount of Dhh1p associated with our OPT and NON-OPT mRNA reporters using an affinity pull-down approach (Figure 3A). Specifically, we treated cells with a low level of formaldehyde to crosslink RNA to associated proteins. We prepared cell lysates and hybridized the mRNA samples to DNA oligonucleotides conjugated to biotin that are antisense to the common 3′ UTR of the OPT and NON-OPT reporters. Following hybridization, ribonucleoprotein (RNP) complexes were affinity purified using magnetic streptavidin beads. Bound material was stringently washed, and elution was then performed using a low-salt buffer. This approach was able to greatly enrich reporter mRNAs relative to an endogenous *PGK1* mRNA (Figure 3B). Moreover, analysis of Dhh1p bound to reporter mRNA by western blot revealed a 3-fold enrichment of Dhh1p on the NON-OPT mRNA relative to the OPT mRNA. As a control, we found that the concentration of poly(A)-binding protein (Pab1p) isolated on both mRNAs was equal (Figure 3C); as anticipated, we found no discernible GAPDH associated with either mRNP.

We extended this reporter analysis to define the association of Dhh1p with all mRNA transcripts on a genome-wide basis. Previous crosslinking and immunoprecipitation (CLIP) studies found that Dhh1p bound throughout the 5′ and 3′ UTRs and the open reading frame (ORF) of most genes with no discernible binding motif and little apparent enrichment in any particular region of the transcript. We used the same published Dhh1p CLIP data (Mitchell et al., 2013) and asked whether association of Dhh1p was governed by the optimality of the transcript. In both replicates of the CLIP experiment, we see that Dhh1p is preferentially bound to low sTAI genes relative to higher sTAI genes (Figure 3D).

The Number of Slow-Moving Ribosomes Stimulates mRNA Decay

We have previously demonstrated that the ratio of optimal to non-optimal codons is a key determinant in mRNA half-lives (Presnyak et al., 2015). Here, we have shown that Dhh1p selectively binds mRNAs of low codon optimality and is critical in dictating codon-defined mRNA stability. A parsimonious explanation for these observations is that the density of slow-moving ribosomes on an mRNA (dictated by codon optimality) is sensed by Dhh1p and communicated to the mRNA degradation machinery. We tested this idea by generating a series of reporters based on the highly optimal *PGK1* mRNA, where into each derivative we placed an identical stretch of ten amino acids of exceptionally low sTAI (sTAI = 0.101) at increasing distances from the initiating AUG (5%, 25%, 50%, 63%, and 77% away) (Figure 4A). Importantly, the non-optimal codon (NC) stretch is of sufficiently low sTAI that it is predicted to dramatically slow ribosomes at the site and in turn upstream; we see that protein expression is strongly and equivalently reduced for all five constructs to ~10% of that of the normal *PGK1* mRNA (Figure S3A). As before, we monitored the mRNA half-lives of these reporters using a

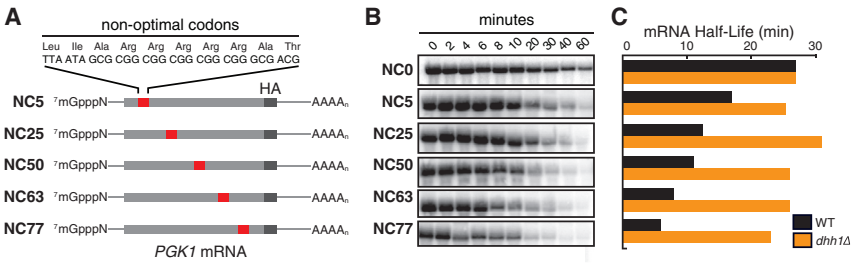

Figure 4. Dhh1p Senses the Polarity of a Stretch of Non-optimal Codons in an Optimal mRNA

(A) Representation of *PGK1* reporters with a stretch of ten non-optimal codons at increasing distances from the initiating AUG. NC, non-optimal codons; NC0, no stretch; NC5, 25, 50, 63, 77, non-optimal codon stretch 5%, 25%, 50%, 63%, and 77% away from the AUG.

(B) Northern blots of the different *PGK1* reporters after GAL-transcriptional shutoff showing the remaining mRNA at the indicated time-points after shutoff.

(C) Half-lives of the different *PGK1* reporters calculated from the northern blots (quantitation was normalized to *SCR1*, and loading controls are not shown) in WT and *dhh1Δ* cells.

See also Figure S3.

GAL-transcriptional shutoff approach. We observed a striking polarity for the overall half-lives of the mRNAs that scaled with the distance of the NC stretch from the AUG. Importantly, the polarity of RNA decay was abrogated on deletion of *DHH1* (Figure 4C). The least stable mRNA reporters are those with the NC stretch the furthest from the AUG start site, where the maximal number of ribosomes would likely have accumulated on the ORF. These data indicate that the number of slow-moving (or stalled) ribosomes is at a minimum correlated with the half-life of the mRNA.

First, we verified that the polarity effect that we observed was dependent on mRNA translation by inserting a stem-loop inhibitory to translational initiation in the 5′ UTR (Figure 5A); indeed, inhibition of translation by the stem loop abrogated the influence of the NC stretch on mRNA decay (Figure 5B). Second, we determined if the polarity effect resulted from ribosome events occurring upstream of the NC stretch or downstream. This idea was tested by placing a premature termination codon immediately after the NC stretch, such that once termination has occurred, ribosomes will no longer be associated downstream of the STOP codon (it follows that these ORFs are now very different in size) (Figure 5C). In a WT yeast background, these reporters exhibit an inverse polarity for their stability, as anticipated from the impact of the nonsense-mediated decay (NMD) pathway on their stability. However, when these same reporters are evaluated in a *upf1Δ* background, we see that the polarity of mRNA degradation is preserved (Figure 5D). These data are consistent with models suggesting that ribosomes stacked upstream of slow codon regions are critical to defining the stability of the various reporter mRNAs.

Lastly, there are numerous quality control (QC) mechanisms that exist within the cell to monitor aberrant translation events (Shoemaker and Green, 2012). As it is formally possible that one of these QC pathways might recognize ribosomes stalled at non-optimal codons as aberrant, we asked whether the polarity effects that we observed resulted from the action of these pathways by performing the same analyses in different mutant backgrounds (*dom34Δ*, *ltn1Δ*, *rqc1Δ*, and *hel2Δ*). Reassuringly, none of these components were observed to impact the polarity of mRNA decay observed in the reporter constructs (Figure S3B).

Collectively, these data indicate that the polarity of mRNA degradation is translation dependent and depends on ribosome-associated events localized between the AUG start site and the NC stretch. The simplest explanation for these observations is that the number of slow-moving ribosomes on an mRNA determines the level of mRNA degradation observed.

Dhh1p Binds Physically to the Eukaryotic Ribosome

While CLIP data suggest that Dhh1p may directly bind to mRNA, thus dictating downstream functional consequences, it seems possible that like other DEAD-box proteins (Geissler et al., 2012; Gingras et al., 1999), Dhh1p could also interact directly with the ribosome to mediate function. We tested this hypothesis by using a tandem-affinity tag (TAP) to purify Dhh1p from yeast cells and identify associated complexes by mass spectrometry. Importantly, we observed eight prominent protein bands upon purification that we identified as ribosomal proteins (Figure 6A). The association with Dhh1p with the ribosome was RNase A insensitive, suggesting a direct ribosome association (data not shown). We next repeated our TAP purification and probed for specific RNA species by northern blot. We observe that both the 25S and 18S rRNAs co-purify with Dhh1p, while other transcripts such as the 7S RNA (*SCR1*) or tRNA do not. Together, these data indicate that Dhh1p physically interacts with the ribosome.

Ribosome Occupancy Is Enhanced when Dhh1p Is Bound

Given the connection that we have established between ribosome density and Dhh1p function in mRNA decay, we next asked whether on a global scale there is preferential effect of Dhh1p on the ribosome occupancy on mRNAs of low codon optimality. Ribosome profiling was performed in four *S. cerevisiae* strains: wild-type, *dhh1Δ*, and constitutively overexpressed (OE) Dhh1p(OE) and Dhh1p-DQAD(OE). The DQAD allele has been previously shown to render Dhh1p nonfunctional (Coller and Parker, 2005). While an assessment of ribosome occupancy (the average number of ribosomes on a given transcript) between the four strains failed to reveal genes or ontological categories of interest, characterizing genes binned according to their overall optimality (sTAI) revealed interesting features. In the Dhh1p(OE) strain, we see a clear pattern of increased ribosome occupancy on non-optimal genes (Figure 6B). As a control, we performed a similar analysis, measuring ribosome occupancy changes in the Dhh1p(OE) strain relative to the catalytically inactive Dhh1p protein (Dhh1p-DQAD(OE)). Again, we observe enrichment of ribosomes on low-optimality mRNAs,

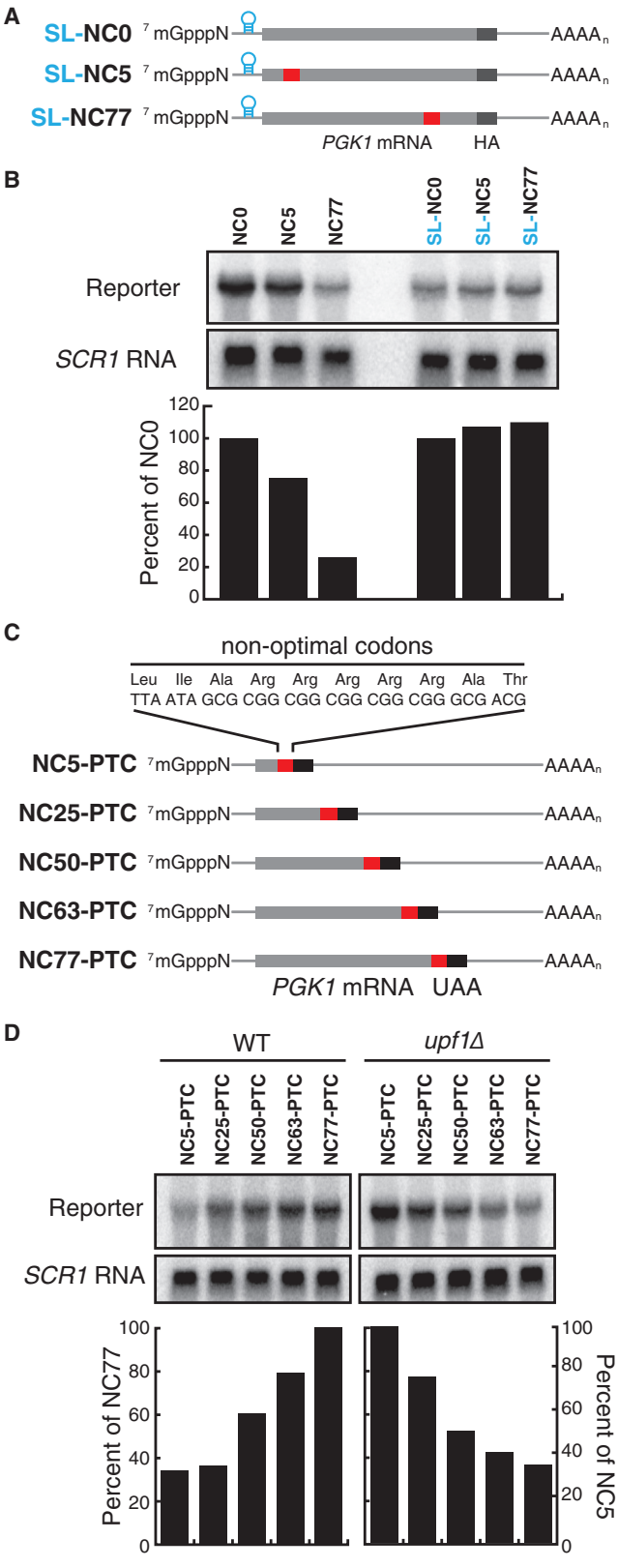

Figure 5. Dhh1p-Mediated Degradation Is Dependent on Inefficient Translation

(A) A stem loop (SL) was inserted in the 5′ UTR of the previously described *PGK1* reporters containing non-optimal codons at variable positions to inhibit translation.

(B) Northern blot for steady-state abundance of the reporters with and without SL, with relative levels shown below. *SCR1* was probed as a loading control.

(C) A premature termination codon (PTC) was inserted immediately after the NC stretch of the reporters to prevent ribosome association downstream of the stretch.

(D) Northern blot for steady-state abundance of the reporters with and without PTC, and relative levels are shown below. *SCR1* was probed as a loading control.

See also Figure S3.

suggesting that this differential ribosome occupancy is dependent on the catalytic activity of Dhh1p (Figure S4A).

We next took advantage of the nucleotide resolution of ribosome footprint profiling to see if increased occupancy on non-optimal genes could be resolved at the codon level. To perform this analysis, we looked at a subset of the reads from footprint profiling (28-nt fragments) in the mutant and wild-type strains to characterize A-site occupancy. We find that when Dhh1p is overexpressed, relative to wild-type, there is increased footprint density when non-optimal codons occupy the A site (Figure 6C); no trends based on codon optimality are seen in the *dhh1Δ* strain.

We additionally profiled strains carrying tethered-reporter constructs similar to those previously characterized (Sweet et al., 2012). Here, we use an mCherry reporter RNA (sTAI = 0.422) tethered through a BoxB-Lambda N system to either Dhh1p or Dhh1p-DQAD (Franklin, 1985a, 1985b; Lazinski et al., 1989). The Dhh1p-tethered mCherry reporter mRNA exhibits 2.7-fold greater ribosome occupancy than the Dhh1p-DQAD tethered reporter (Figure S4B), with reads distributed throughout the ORF. These data are consistent with the global analysis above and with earlier polysome profiling analysis (Sweet et al., 2012).

We next probed the connections among ribosome occupancy, Dhh1p function, and codon optimality. We employed a similar tethering experiment but using instead a short ORF (*OST4*) construct designed to allow for high-resolution sucrose-gradient analysis (Figure 6D). We made synonymous variants of this *OST4* ORF with either high optimality (sTAI = 0.454) or low optimality (sTAI = 0.203) and evaluated its association with polysomes. With this refinement, we could see differences in ribosome occupancy on ORFs as a function of codon optimality. Consistent with our model, we see a clear increase in ribosome occupancy on the HA-OST4-NON-OPT mRNA relative to the HA-OST4-OPT mRNA, dependent on the presence of functional Dhh1p (Figure 6E).

DISCUSSION

It is well established that mRNA translation and mRNA stability are tightly coupled events, although it is unclear at a molecular level how these processes are connected. Recently, we established that codon usage strongly impacts both mRNA stability

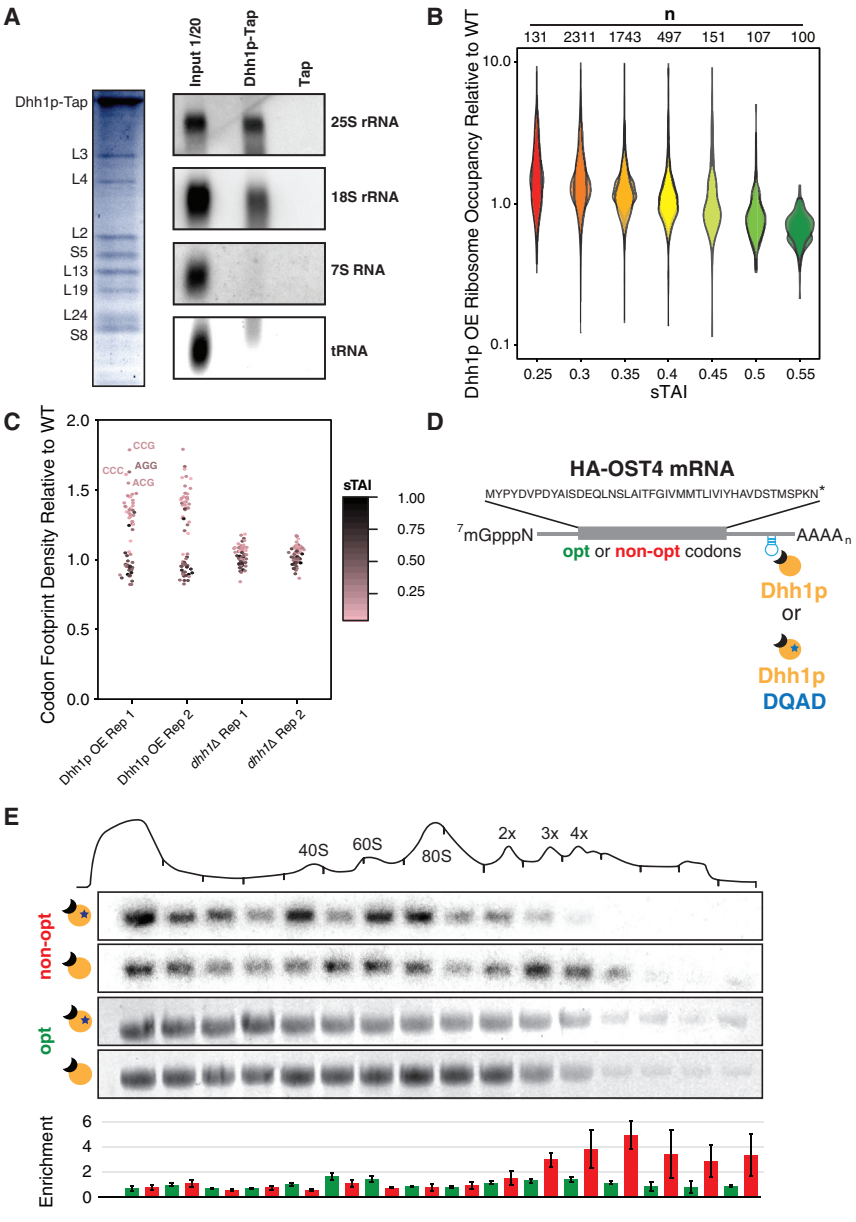

Figure 6. Dhh1p Binds Ribosomes and Preferentially Modulates Ribosome Occupancy on mRNAs with Low Codon Optimality

(A) Dhh1p-TAP purification followed by mass spectrometry (left, Coomassie blue gel staining) or northern blots and specific probing for different rRNAs or tRNA (right).

(B) Plotting the ribosome occupancy (average number of ribosomes per mRNA) for transcripts under constitutive Dhh1p OE relative to WT conditions, binning transcripts by sTAI. Shown are two biological replicates. A two-tailed Mann-Whitney test shows that low-optimality mRNAs (sTAI = 0.25, Med. = 1.30) have increased ribosome occupancy relative to high-optimality mRNAs (sTAI = 0.55, Med. = 0.72) ($U = 1364$, $p < 2.2 \times 10^{-16}$) upon Dhh1p overexpression.

(C) Quantifying the ribosome footprint density in the A site under Dhh1p OE or *dhh1Δ* relative to WT. The identity of the codon in the A site was determined by using 28-nt fragments as outlined previously (Ingolia et al., 2009).

(D) Schematic of the reporter used in polysome occupancy assays.

(E) Northern blots were used to quantify the enrichment (relative fractional occupancy) of optimal and non-optimal HA-OST4 mRNA along a polysome gradient upon tethering catalytically active and inactive Dhh1p. Reported values are averaged across three samples and presented with SE. Shown are representative northern blots for the non-optimal and optimal mRNAs upon tethering of catalytically active and inactive Dhh1p.

See also Figure S4.

Dhh1p and Homologs Are Implicated in Translational Control

A role for Dhh1p in regulating translation elongation is consistent with observations from other systems. For instance, in *Drosophila*, translationally repressed *oskar* and *nanos* mRNAs are found on polyribosomes in a so-called masked state; the Dhh1p-homolog Me31b is required for their masking (Braat et al., 2004; Clark et al., 2000; Nakamura et al., 2001). Similarly, the fragile X mental retardation protein (FMRP), a polysome-associated neuronal RNA binding protein that interacts with Me31b (Barbee et al., 2006), was recently found to regulate translation by inducing stalling of ribosomes on target mRNAs (Darnell et al., 2011). Given the high conservation and essential nature of Dhh1p in higher eukaryotes, it seems likely that such a critical role in modulating translational elongation is conserved throughout the eukaryotic lineage.

Dhh1p and homologs have also been implicated in the regulation of translational initiation. Recombinant Dhh1p in high concentrations inhibits 48S ribosome initiation complex formation in vitro (Coller and Parker, 2005). Moreover, multiple recent studies interested in miRNA-mediated regulation have implicated the mammalian Dhh1p homolog, DDX6, in interactions with the CCR4-NOT complex relevant to translational silencing and translational elongation (Presnyak et al., 2015). In this study, we provide a mechanistic understanding of how the rates of translation are communicated to the mRNA degradation apparatus. We propose that the decapping activator and translational regulator Dhh1p is a sensor of ribosome speed across the transcriptome (Figure 7). We hypothesize that Dhh1p dynamically samples elongation events, binding to the translating mRNPs when elongation is slow. Dhh1p's association with the translating mRNP may act to slow ribosome movement even further, suggesting an active rather than passive role in coupling translation repression to decay; however, further studies are required to glean mechanistic insight. Ultimately, Dhh1p's association with the translating mRNP leads to activation of mRNA decapping and degradation.

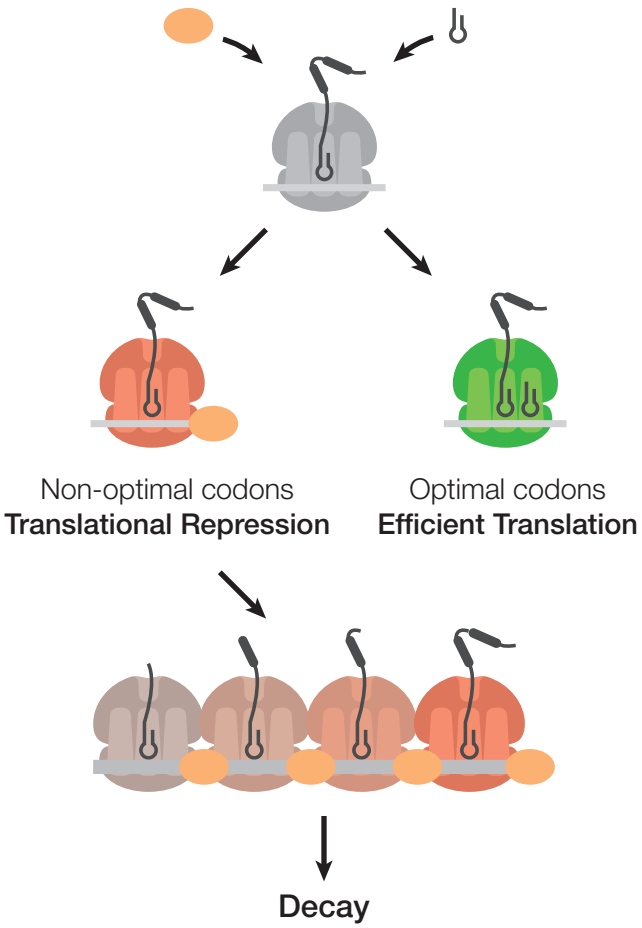

Figure 7. Model: Dhh1p Is a General and Essential Sensor of Ribosome Speed during Elongation

In this model, codon optimality influences the transit speed of ribosomes which in turns affects the association of the decay factor Dhh1p. Ribosomes are slowed down on non-optimal stretches, recruiting Dhh1p, which may further slow ribosome movement and leads to mRNA decapping and degradation.

(Chen et al., 2014; Mathys et al., 2014; Ozgur et al., 2015; Rouya et al., 2014); there is emerging consensus in this field that translational inhibition in these systems is imposed at the initiation step (Fabian and Sonenberg, 2012).

A role for Dhh1p in controlling translational initiation and elongation need not be mutually exclusive. Indeed, we have documented that Dhh1p contacts the ribosome. Thus, the regulation of both elongation and initiation by Dhh1p may be a manifestation of the same molecular contacts with the ribosome itself. The seemingly distinct cellular responses may simply depend on the relative concentrations of the factor and the state of the ribosome being accessed (the kinetics and thermodynamics of the event). In higher eukaryotes, recent findings suggest that the basis for these disparate cellular roles may lie in the complex macromolecular associations that the DDX6-CCR4-NOT complex makes with downstream effector proteins (Ozgur et al., 2015). Detailed understanding of the molecular contacts of Dhh1p with the ribosome may ultimately reconcile these apparent discrepancies.

Normal mRNA Decay Is a Response to Subtle Changes in Translation Rate

It is well established that the ribosome is centrally involved in specifying mRNA degradation on aberrant transcripts. The processes of NMD, no-go decay (NGD), and non-stop decay (NSD) all are dictated by abnormal events on the ribosome within the ribosomal A site (i.e., a premature termination codon, a truncated mRNA, or a string of AAA [lysine] codons) (Shoemaker and Green, 2012). Importantly, however, a direct connection between ribosome function and normal mRNA decay has not been established. Our data here provide clear evidence for an intimate connection between efficient translation of mRNAs by ribosomes and normal mRNA decay mediated by the DEAD-box protein Dhh1p. Given that the main function of an mRNA is the production of protein product through translation, such a central role for the ribosome in specifying its stability is reassuring.

STAR★METHODS

Detailed methods are provided in the online version of this paper and include the following:

- KEY RESOURCES TABLE
- CONTACT FOR REAGENT AND RESOURCE SHARING
- EXPERIMENTAL MODEL AND SUBJECT DETAILS
  - Yeast Strains and Growth Conditions
- METHOD DETAILS
  - Plasmids, Oligonucleotides and Strain Construction
  - Transcriptional Shutoffs and Steady State RNA Northern Blot Analysis
  - Protein Isolation and Western Blot Analysis
  - mRNA Pull-Down
  - Tandem Affinity Purification
  - Northern Blots of Constructs across Sucrose Gradients
  - Preparation of Footprint and RNA-Seq Libraries
  - Read Preparation and Sequence Alignment
- QUANTIFICATION AND STATISTICAL ANALYSIS
- DATA AND SOFTWARE AVAILABILITY
  - Data Resources

SUPPLEMENTAL INFORMATION

Supplemental Information includes four figures and four tables and can be found with this article online at http://dx.doi.org/10.1016/j.cell.2016.08.053.

AUTHOR CONTRIBUTIONS

A.R., R.G., and J.C. wrote the manuscript. A.R., Y.-H.C., N.A., and S.M. performed the experiments. All authors contributed to the discussion and design of this research. All authors commented on the manuscript.

ACKNOWLEDGMENTS

We thank Wenqian Hu, Vlad Presnyak, Carrie Kovalak, Lisa Lojek, Jenna Smith, Kristian Baker, Boris Zinshteyn, Nick Guydosh, and Kristin Smith-Koutmos for productive discussions and technical assistance during this study. Funding was provided by the National Institutes of Health (J.C. and R.G.) and the Howard Hughes Medical Institute (R.G.).

Received: December 18, 2015
Revised: April 25, 2016
Accepted: August 19, 2016
Published: September 15, 2016

REFERENCES

Anderson, J.S., and Parker, R.P. (1998). The 3′ to 5′ degradation of yeast mRNAs is a general mechanism for mRNA turnover that requires the SKI2 DEVH box protein and 3′ to 5′ exonucleases of the exosome complex. EMBO J. *17*, 1497–1506.

Barbee, S.A., Estes, P.S., Cziko, A.M., Hillebrand, J., Luedeman, R.A., Coller, J.M., Johnson, N., Howlett, I.C., Geng, C., Ueda, R., et al. (2006). Staufen- and FMRP-containing neuronal RNPs are structurally and functionally related to somatic P bodies. Neuron *52*, 997–1009.

Boël, G., Letso, R., Neely, H., Price, W.N., Wong, K.H., Su, M., Luff, J.D., Valecha, M., Everett, J.K., Acton, T.B., et al. (2016). Codon influence on protein expression in E. coli correlates with mRNA levels. Nature *529*, 358–363.

Braat, A.K., Yan, N., Arn, E., Harrison, D., and Macdonald, P.M. (2004). Localization-dependent oskar protein accumulation; control after the initiation of translation. Dev. Cell *7*, 125–131.

Bulmer, M., Wolfe, K.H., and Sharp, P.M. (1991). Synonymous nucleotide substitution rates in mammalian genes: implications for the molecular clock and the relationship of mammalian orders. Proc. Natl. Acad. Sci. USA *88*, 5974–5978.

Carroll, J.S., Munchel, S.E., and Weis, K. (2011). The DExD/H box ATPase Dhh1 functions in translational repression, mRNA decay, and processing body dynamics. J. Cell Biol. *194*, 527–537.

Charneski, C.A., and Hurst, L.D. (2013). Positively charged residues are the major determinants of ribosomal velocity. PLoS Biol. *11*, e1001508.

Chen, Y., Boland, A., Kuzuoğlu-Öztürk, D., Bawankar, P., Loh, B., Chang, C.T., Weichenrieder, O., and Izaurralde, E. (2014). A DDX6-CNOT1 complex and W-binding pockets in CNOT9 reveal direct links between miRNA target recognition and silencing. Mol. Cell *54*, 737–750.

Clark, I.E., Wyckoff, D., and Gavis, E.R. (2000). Synthesis of the posterior determinant Nanos is spatially restricted by a novel cotranslational regulatory mechanism. Curr. Biol. *10*, 1311–1314.

Coller, J., and Parker, R. (2005). General translational repression by activators of mRNA decapping. Cell *122*, 875–886.

Coller, J.M., Tucker, M., Sheth, U., Valencia-Sanchez, M.A., and Parker, R. (2001). The DEAD box helicase, Dhh1p, functions in mRNA decapping and interacts with both the decapping and deadenylase complexes. RNA *7*, 1717–1727.

Dana, A., and Tuller, T. (2014). The effect of tRNA levels on decoding times of mRNA codons. Nucleic Acids Res. *42*, 9171–9181.

Darnell, J.C., Van Driesche, S.J., Zhang, C., Hung, K.Y., Mele, A., Fraser, C.E., Stone, E.F., Chen, C., Fak, J.J., Chi, S.W., et al. (2011). FMRP stalls ribosomal translocation on mRNAs linked to synaptic function and autism. Cell *146*, 247–261.

Decker, C.J., and Parker, R. (1993). A turnover pathway for both stable and unstable mRNAs in yeast: evidence for a requirement for deadenylation. Genes Dev. *7*, 1632–1643.

Dix, D.B., and Thompson, R.C. (1989). Codon choice and gene expression: synonymous codons differ in translational accuracy. Proc. Natl. Acad. Sci. USA *86*, 6888–6892.

Dong, H., Nilsson, L., and Kurland, C.G. (1996). Co-variation of tRNA abundance and codon usage in Escherichia coli at different growth rates. J. Mol. Biol. *260*, 649–663.

dos Reis, M., Savva, R., and Wernisch, L. (2004). Solving the riddle of codon usage preferences: a test for translational selection. Nucleic Acids Res. *32*, 5036–5044.

Drummond, D.A., and Wilke, C.O. (2008). Mistranslation-induced protein misfolding as a dominant constraint on coding-sequence evolution. Cell *134*, 341–352.

Fabian, M.R., and Sonenberg, N. (2012). The mechanics of miRNA-mediated gene silencing: a look under the hood of miRISC. Nat. Struct. Mol. Biol. *19*, 586–593.

Fischer, N., and Weis, K. (2002). The DEAD box protein Dhh1 stimulates the decapping enzyme Dcp1. EMBO J. *21*, 2788–2797.

Franklin, N.C. (1985a). Conservation of genome form but not sequence in the transcription antitermination determinants of bacteriophages lambda, phi 21 and P22. J. Mol. Biol. *181*, 75–84.

Franklin, N.C. (1985b). "N" transcription antitermination proteins of bacteriophages lambda, phi 21 and P22. J. Mol. Biol. *181*, 85–91.

Gardin, J., Yeasmin, R., Yurovsky, A., Cai, Y., Skiena, S., and Futcher, B. (2014). Measurement of average decoding rates of the 61 sense codons in vivo. eLife *3*, e03735.

Geissler, R., Golbik, R.P., and Behrens, S.E. (2012). The DEAD-box helicase DDX3 supports the assembly of functional 80S ribosomes. Nucleic Acids Res. *40*, 4998–5011.

Ghaemmaghami, S., Huh, W.K., Bower, K., Howson, R.W., Belle, A., Dephoure, N., O'Shea, E.K., and Weissman, J.S. (2003). Global analysis of protein expression in yeast. Nature *425*, 737–741.

Gingold, H., and Pilpel, Y. (2011). Determinants of translation efficiency and accuracy. Mol. Syst. Biol. *7*, 481.

Gingras, A.C., Raught, B., and Sonenberg, N. (1999). eIF4 initiation factors: effectors of mRNA recruitment to ribosomes and regulators of translation. Annu. Rev. Biochem. *68*, 913–963.

Guydosh, N.R., and Green, R. (2014). Dom34 rescues ribosomes in 3′ untranslated regions. Cell *156*, 950–962.

Hershberg, R., and Petrov, D.A. (2008). Selection on codon bias. Annu. Rev. Genet. *42*, 287–299.

Hsu, C.L., and Stevens, A. (1993). Yeast cells lacking 5′–>3′ exoribonuclease 1 contain mRNA species that are poly(A) deficient and partially lack the 5′ cap structure. Mol. Cell. Biol. *13*, 4826–4835.

Hu, W., Sweet, T.J., Chamnongpol, S., Baker, K.E., and Coller, J. (2009). Co-translational mRNA decay in Saccharomyces cerevisiae. Nature *461*, 225–229.

Hussmann, J.A., Patchett, S., Johnson, A., Sawyer, S., and Press, W.H. (2015). Understanding Biases in Ribosome Profiling Experiments Reveals Signatures of Translation Dynamics in Yeast. PLoS Genet. *11*, e1005732.

Ikemura, T., and Ozeki, H. (1983). Codon usage and transfer RNA contents: organism-specific codon-choice patterns in reference to the isoacceptor contents. Cold Spring Harb. Symp. Quant. Biol. *47*, 1087–1097.

Ingolia, N.T., Ghaemmaghami, S., Newman, J.R., and Weissman, J.S. (2009). Genome-wide analysis in vivo of translation with nucleotide resolution using ribosome profiling. Science *324*, 218–223.

Ingolia, N.T., Lareau, L.F., and Weissman, J.S. (2011). Ribosome profiling of mouse embryonic stem cells reveals the complexity and dynamics of mammalian proteomes. Cell *147*, 789–802.

Kim, S.J., Yoon, J.S., Shishido, H., Yang, Z., Rooney, L.A., Barral, J.M., and Skach, W.R. (2015). Protein folding. Translational tuning optimizes nascent protein folding in cells. Science *348*, 444–448.

Langmead, B., Trapnell, C., Pop, M., and Salzberg, S.L. (2009). Ultrafast and memory-efficient alignment of short DNA sequences to the human genome. Genome Biol. *10*, R25.

Lazinski, D., Grzadzielska, E., and Das, A. (1989). Sequence-specific recognition of RNA hairpins by bacteriophage antiterminators requires a conserved arginine-rich motif. Cell *59*, 207–218.

Li, G.W., Oh, E., and Weissman, J.S. (2012). The anti-Shine-Dalgarno sequence drives translational pausing and codon choice in bacteria. Nature *484*, 538–541.

Longtine, M.S., McKenzie, A., 3rd, Demarini, D.J., Shah, N.G., Wach, A., Brachat, A., Philippsen, P., and Pringle, J.R. (1998). Additional modules for

versatile and economical PCR-based gene deletion and modification in Saccharomyces cerevisiae. Yeast *14*, 953–961.

Man, O., and Pilpel, Y. (2007). Differential translation efficiency of orthologous genes is involved in phenotypic divergence of yeast species. Nat. Genet. *39*, 415–421.

Martin, M. (2011). Cutadapt removes adapter sequences from high-throughput sequencing reads. EMBnet.journal *17*, 10–12.

Mathys, H., Basquin, J., Ozgur, S., Czarnocki-Cieciura, M., Bonneau, F., Aartse, A., Dziembowski, A., Nowotny, M., Conti, E., and Filipowicz, W. (2014). Structural and biochemical insights to the role of the CCR4-NOT complex and DDX6 ATPase in microRNA repression. Mol. Cell *54*, 751–765.

Mishima, Y., and Tomari, Y. (2016). Codon usage and 3′ UTR length determine maternal mRNA stability in zebrafish. Mol. Cell *61*, 874–885.

Mitchell, S.F., Jain, S., She, M., and Parker, R. (2013). Global analysis of yeast mRNPs. Nat. Struct. Mol. Biol. *20*, 127–133.

Muhlrad, D., Decker, C.J., and Parker, R. (1994). Deadenylation of the unstable mRNA encoded by the yeast MFA2 gene leads to decapping followed by 5′–>3′ digestion of the transcript. Genes Dev. *8*, 855–866.

Nakamura, A., Amikura, R., Hanyu, K., and Kobayashi, S. (2001). Me31B silences translation of oocyte-localizing RNAs through the formation of cytoplasmic RNP complex during Drosophila oogenesis. Development *128*, 3233–3242.

Novoa, E.M., and Ribas de Pouplana, L. (2012). Speeding with control: codon usage, tRNAs, and ribosomes. Trends Genet. *28*, 574–581.

Ozgur, S., Basquin, J., Kamenska, A., Filipowicz, W., Standart, N., and Conti, E. (2015). Structure of a human 4E-T/DDX6/CNOT1 complex reveals the different interplay of DDX6-binding proteins with the CCR4-NOT complex. Cell Rep. *13*, 703–711.

Pechmann, S., and Frydman, J. (2013). Evolutionary conservation of codon optimality reveals hidden signatures of cotranslational folding. Nat. Struct. Mol. Biol. *20*, 237–243.

Pelechano, V., Wei, W., and Steinmetz, L.M. (2015). Widespread Co-translational RNA Decay Reveals Ribosome Dynamics. Cell *161*, 1400–1412.

Pop, C., Rouskin, S., Ingolia, N.T., Han, L., Phizicky, E.M., Weissman, J.S., and Koller, D. (2014). Causal signals between codon bias, mRNA structure, and the efficiency of translation and elongation. Mol. Syst. Biol. *10*, 770.

Presnyak, V., and Coller, J. (2013). The DHH1/RCKp54 family of helicases: an ancient family of proteins that promote translational silencing. Biochim. Biophys. Acta *1829*, 817–823.

Presnyak, V., Alhusaini, N., Chen, Y.H., Martin, S., Morris, N., Kline, N., Olson, S., Weinberg, D., Baker, K.E., Graveley, B.R., and Coller, J. (2015). Codon optimality is a major determinant of mRNA stability. Cell *160*, 1111–1124.

Rigaut, G., Shevchenko, A., Rutz, B., Wilm, M., Mann, M., and Séraphin, B. (1999). A generic protein purification method for protein complex characterization and proteome exploration. Nat. Biotechnol. *17*, 1030–1032.

Rocha, E.P. (2004). Codon usage bias from tRNA's point of view: redundancy, specialization, and efficient decoding for translation optimization. Genome Res. *14*, 2279–2286.

Rouya, C., Siddiqui, N., Morita, M., Duchaine, T.F., Fabian, M.R., and Sonenberg, N. (2014). Human DDX6 effects miRNA-mediated gene silencing via direct binding to CNOT1. RNA *20*, 1398–1409.

Sabi, R., and Tuller, T. (2014). Modelling the efficiency of codon-tRNA interactions based on codon usage bias. DNA Res. *21*, 511–526.

Sander, I.M., Chaney, J.L., and Clark, P.L. (2014). Expanding Anfinsen's principle: contributions of synonymous codon selection to rational protein design. J. Am. Chem. Soc. *136*, 858–861.

Shoemaker, C.J., and Green, R. (2012). Translation drives mRNA quality control. Nat. Struct. Mol. Biol. *19*, 594–601.

Sørensen, M.A., Kurland, C.G., and Pedersen, S. (1989). Codon usage determines translation rate in Escherichia coli. J. Mol. Biol. *207*, 365–377.

Spencer, P.S., Siller, E., Anderson, J.F., and Barral, J.M. (2012). Silent substitutions predictably alter translation elongation rates and protein folding efficiencies. J. Mol. Biol. *422*, 328–335.

Sweet, T., Kovalak, C., and Coller, J. (2012). The DEAD-box protein Dhh1 promotes decapping by slowing ribosome movement. PLoS Biol. *10*, e1001342.

Thomas, L.K., Dix, D.B., and Thompson, R.C. (1988). Codon choice and gene expression: synonymous codons differ in their ability to direct aminoacylated-transfer RNA binding to ribosomes in vitro. Proc. Natl. Acad. Sci. USA *85*, 4242–4246.

Tuller, T., Waldman, Y.Y., Kupiec, M., and Ruppin, E. (2010). Translation efficiency is determined by both codon bias and folding energy. Proc. Natl. Acad. Sci. USA *107*, 3645–3650.

Varenne, S., Buc, J., Lloubes, R., and Lazdunski, C. (1984). Translation is a non-uniform process. Effect of tRNA availability on the rate of elongation of nascent polypeptide chains. J. Mol. Biol. *180*, 549–576.

Weinberg, D.E., Shah, P., Eichhorn, S.W., Hussmann, J.A., Plotkin, J.B., and Bartel, D.P. (2016). Improved ribosome-footprint and mRNA measurements provide insights into dynamics and regulation of yeast translation. Cell Rep. *14*, 1787–1799.

Yu, C.H., Dang, Y., Zhou, Z., Wu, C., Zhao, F., Sachs, M.S., and Liu, Y. (2015). Codon usage influences the local rate of translation elongation to regulate co-translational protein folding. Mol. Cell *59*, 744–754.

Zhang, G., Hubalewska, M., and Ignatova, Z. (2009). Transient ribosomal attenuation coordinates protein synthesis and co-translational folding. Nat. Struct. Mol. Biol. *16*, 274–280.

STAR★METHODS

KEY RESOURCES TABLE

REAGENT or RESOURCE	SOURCE	IDENTIFIER
Antibodies		
Mouse monoclonal anti-HA	BioLegend	Cat#901503; RRID:AB_2565005
Mouse monoclonal anti-PAB1	EnCor Biotechnology	Cat#MCA-1G1; RRID:AB_2572370
Mouse monoclonal anti-GAPDH	Cell Biolabs	Cat#AKR-001
Chemicals, Peptides, and Recombinant Proteins		
Cycloheximide	Sigma-Aldrich	C1988; CAS: 66-81-9
Heparin	Sigma-Aldrich	H3393; CAS: 9041-08-1
SuperaseIn	Ambion	AM2694
RNase I	Ambion	AM2294
T4 Polynucleotide Kinase	New England Biosciences	M0201L
T4 RNA Ligase 2, Truncated	New England Biosciences	M0242L
Superscript III	Invitrogen	56575
GlycoBlue	ThermoFisher	AM9515
Streptavidin Dynabeads	Invitrogen	65002
Protease Inhibitor Cocktail	Sigma-Aldrich	P8215
Sepharose 6B beads	Sigma-Aldrich	6B100
IgG Sepharose 6 Fast Flow	GE Healthcare	17-0969-01
AcTEV-protease	Invitrogen	12575-015
Calmodulin Sepharose	GE Healthcare	17-0529-01
Critical Commercial Assays		
Ribo-Zero Gold rRNA Removal Kit (Yeast)	Illumina	MRZY1306
CircLigase ssDNA Ligase	Epicenter	CL4115K
Deposited Data		
Raw and analyzed data	This paper	GEO: GSE81269
Dhh1p CLIP Sequencing	Mitchell et al., 2013	GEO: GSE46142
R64-1-1 S288C sacCer3 Genome Assembly	*Saccharomyces* Genome Database Project	http://downloads.yeastgenome.org/sequence/S288C_reference/genome_releases/
Yeast ncRNA Gene Database	*Saccharomyces* Genome Database Project	http://downloads.yeastgenome.org/sequence/S288C_reference/rna/archive/rna_coding_R64-1-1_20110203.fasta.gz
Experimental Models: Organisms/Strains		
See Table S2 for a list of strains used in this study	This paper	N/A
Recombinant DNA		
See Table S4 for a list of plasmids used in this study	This paper	N/A
Sequence-Based Reagents		
See Table S3 for a list of oligonucleotides used in this study	This paper	N/A
Software and Algorithms		
Bowtie	Langmead et al., 2009	http://bowtie-bio.sourceforge.net
ImageQuant	GE Healthcare	TL 5.2
ImageJ	NIH, USA	https://imagej.nih.gov/ij
CutAdapt	Martin, 2011	https://cutadapt.readthedocs.io/en/stable/
Other		
Analysis and scripts of deep sequencing data (Pipeline.py, DataGen.py, Plot.R)	This paper	https://github.com/greenlabjhmi/2016-Cell-Dhh1

CONTACT FOR REAGENT AND RESOURCE SHARING

Please direct any requests for further information or reagents to the lead contact, Jeff Coller (jmc71@case.edu).

EXPERIMENTAL MODEL AND SUBJECT DETAILS

Yeast Strains and Growth Conditions

Yeast strains used in this study are listed in Table S2. All strains, excepting those used for polysome and ribosome profiling, were grown at 24°C in standard synthetic media with the appropriate amino acids and either 2% glucose or 2% galactose/1% sucrose. Cells were harvested at mid-log phase (OD_{600} = 0.4-0.55).

Cells used in polysome profiling were grown in dropout media (CSM –Leu – Ura) and 2% galactose/raffinose at 30°C until mid-log phase (OD_{600} = 0.45-0.5). Cells used in ribosome profiling and RNA-Seq were grown at 30°C in either YPD or CSM – Leu dropout media and with 2% glucose for those transformed with the pAG425 plasmid and CSM –Leu – Ura and 2% galactose/raffinose for those transformed with both the pAG425 and pYES-DEST52 plasmids. Cells were harvested at early-log phase (OD_{600} = 0.3-0.35).

METHOD DETAILS

Plasmids, Oligonucleotides and Strain Construction

All oligonucleotides used in this study are listed in Table S3. All plasmids used in this study are listed in Table S4.

For the *HIS3* constructs with 0%–100% optimality (in 10% increments), oJC2724 to oJC2732 were cloned into pJC716 (Presnyak et al., 2015) using *AscI* and *PacI* restriction sites to create *HIS3* constructs with 10%–90% optimality, respectively. pJC716 (100% optimality), pJC719 (0% optimality, Presnyak et al., 2015), and these 10%–90% optimality constructs were subsequently mutagenized using oJC2857/oJC2858 (pJC716), oJC2861/oJC2862 (40% and 50% optimality), oJC2912/oJC2913 (pJC719), oJC2914/oJC2915 (10% optimality), oJC2916/oJC2917 (20% and 30% optimality) and oJC2918/oJC2919 to oJC2924/oJC2925 (60% to 90% optimality, respectively). The resulting plasmids, pJC797 and pJC800 to pJC809, express N-terminally FLAG-tagged *HIS3* with 0%–100% optimality (in 10% increments). Importantly, a stretch of 23 nucleotides (GGAGTAAAAAGGTTTGGATCAGG) was maintained in all *HIS3* constructs to allow for northern analysis using oligo probe oJC2564.

In order to place the 0%–100% optimality *HIS3* constructs under the control of the *GAL1* promoter, an MluI restriction site was introduced upstream of the *HIS3* 5′ UTR in pJC797 and pJC800 to pJC809 using oJC3083/oJC3084. The *GAL1* promoter (amplified from pFA6a-kanMX6-PGAL1 from (Longtine et al., 1998) using oJC3086/oJC3087) was subsequently cloned into these plasmids using MluI and PacI sites, resulting in the replacement of the *HIS3* 5′ UTR with the *GAL1* promoter and the creation of plasmids pJC857 to pJC867.

To construct the *PGK1*^{NC5}-HA-MS2 reporter containing 10 non-optimal codons 5% away from the initiating AUG (pJC468), DNA was first amplified from pJC296 (*PGK1*-pG, pRP469) (Decker and Parker, 1993) using oligonucleotides oJC558/oJC877 and oJC559/oJC876 then combined and used as the template for amplification of full-length *PGK1* using oligonucleotides oJC558/oJC559. Full-length fragments were cloned into the HindIII and BamHI sites of pJC296 to give pJC399. pJC468 was obtained by inserting HA-MS2 extracted from pJC441 (*PGK1*-HA-MS2, Sweet et al., 2012) into BglII and HindIII of pJC399.

PGK1^{NC25}-HA-MS2 (pJC469), *PGK1*^{NC50}-HA-MS2 (pJC470) and *PGK1*^{NC63}-HA-MS2 (pJC471) were constructed in a similar manner using oJC1261/oJC1244 and oJC1245/oJC559 (pJC469), oJC1261/oJC1246 and oJC1247/oJC559 (pJC470) or oJC1261/oJC1248 and oJC1249/oJC559 (pJC471) and combining the DNA with oJC1261/oJC559 to introduce into the XmaI and HindIII sites of pJC441 (*PGK1*-HA-MS2). *PGK1*^{NC77}-HA-MS2 (pJC443) was obtained by inserting HA sequence into the *AscI* and *PacI* sites (before stop codon) of pJC425 (*PGK1*^{NC77}-MS2, Sweet et al., 2012) using oJC1196/oJC1197. *PGK1*^{NC5}-PTC-HA-MS2 (pJC484), *PGK1*^{NC25}-PTC-HA-MS2 (pJC485), *PGK1*^{NC50}-PTC-HA-MS2 (pJC486), *PGK1*^{NC63}-PTC-HA-MS2 (pJC487) and *PGK1*^{NC77}-PTC-HA-MS2 (pJC488) reporters were obtained by introducing a PTC after the stretch of non-optimal codons by site-directed mutagenesis of the plasmids pJC468 (using oJC1307/oJC1308), pJC469 (using oJC1309/oJC1310), pJC470 (using oJC1311/oJC1312), pJC471 (using oJC1313/oJC1314) and pJC443 (using oJC1315/oJC1316), respectively. pJC134 (SL-*PGK1*, stem-loop containing reporter, Hu et al., 2009) was used to create pJC442 (SL-*PGK1*-HA-MS2, Sweet et al., 2012). SL-*PGK1*^{NC5}-HA-MS2 (pJC497) and SL-*PGK1*^{NC77}-HA-MS2 (pJC498) were obtained by inserting the stretch of non-optimal codons into pJC442, by site-directed mutagenesis using oJC1370/oJC1371/oJC1372/oJC1373 (pJC497) or oJC1374/oJC1375/oJC1376/oJC1377 (pJC498).

To construct the reporters containing the tag sequence (AGATGGTGATGT TAATGGGCAC AAATTTTCTG TCAGTGGAGA GGGTGAAGGT GATGCAACAT ACGGAAAACT TACCCTTAAA TTTATTTGCA CTACTGGAAA ACTACCTGTT CCATGGC) for mRNA pull-down experiment at the 3′-UTR of the plasmids bearing SYN opt RNA (pJC672) and SYN nonopt RNA (pJC673), XhoI and AscI sites were introduced by using oJC2476/oJC2477 and oJC2478/oJC2479 to generate pJC704 and pJC705. tag sequence was amplified from pKB290 with oJC2024/oJC2480, and inserted into the XhoI and AscI site of pJC704 and pJC705 to generate pJC706 and pJC707. These plasmids were transformed into yJC1780 to make yJC2018 and yJC2019.

To construct Dhh1p-TAP for the affinity purification experiments, Dhh1p-TAP sequence was amplified from genomic DNA in YDL160C with oJC126/oJC232 to create pJC223, which was transformed into yJC151 to make yJC335. A control plasmid

expressing TAP only (pJC228) was obtained by deleting Dhh1p from pJC223 after introduction of XhoI sites by site-directed mutagenesis at the AUG and stop codons of Dhh1p (using oJC242/oJC243/oJC244/oJC245). pJC228 was transformed into yJC151 to obtain yJC278.

Transcriptional Shutoffs and Steady State RNA Northern Blot Analysis

For the *rpb1-1* shutoffs, cells were grown at 24°C in synthetic media containing 2% glucose and lacking the appropriate amino acids. Once the cells reached mid-log phase, they were shifted to 37°C to inhibit transcription, and cell aliquots were harvested at the time points indicated in Figure 1.

For the *GAL1* promoter shutoffs and steady state analysis, cells expressing the appropriate plasmids were grown at 24°C in synthetic media with 2% galactose/1% sucrose to allow for expression of the reporter mRNA. For the steady state analysis, cells were harvested at OD_{600} = 0.4. For the transcriptional shutoffs, cells were shifted to synthetic media without sugar at an OD_{600} = 0.4, and then transcription was repressed by adding glucose to a final concentration of 4%. Cells were collected at the time points indicated in the figures.

Total RNA was extracted by phenol/chloroform and precipitated by 95% EtOH. 30-40 μg of RNA was separated on 1.4% agarose-formaldehyde gels, transferred to nylon membranes and probed with ^{32}P-labeled oligonucleotides antisense to *HIS3* (oJC2564), poly (G) (oJC168), MS2 binding sites (oJC1006), *PGK1* (oJC986) or *SCR1* (oJC168). Blots were exposed to PhosphorImager screens, scanned by Typhon 9400, and quantified with ImageQuant software.

Protein Isolation and Western Blot Analysis

Cells were harvested at OD_{600} = 0.4 and protein was isolated by 5M Urea and solution A (125 mM Tris-HCl pH 6.8, 2% SDS). Equivalent OD_{280} unit of protein was separated on 10% SDS polyacrylamide gels, transferred to PVDF membrane, blotted with primary antibodies (anti-HA [BioLegend], anti-Pab1 [EnCor Biotechnology], anti-GAPDH [Cell Biolabs] and anti-Rpl5) at 4°C overnight and incubated with secondary antibodies (goat-anti-Mouse [Santa Cruz sc-2005] and goat-anti-Rabbit [Pierce 31460]) at room temperature for 1 hr. Signal was detected by chemiluminescence using Blue Ultra Autorad film (GeneMate F-2029).

mRNA Pull-Down

Cells (200 ml) were harvested at OD_{600} = 0.4 after crosslinking with 0.25% formaldehyde for 5 min and quenching with 125 mM glycine for 10 min. Cell pellets were lysed in 400 μl 1X polysome lysis buffer (10 mM Tris, pH 7.4, 100 mM NaCl, 30mM MgCl2, 1 mM DTT) by vortexing with glass beads. The hot needle puncture method followed by centrifugation at 2,000 rpm for 2 min at 4°C was used to remove cell debris. Equal OD units (OD260) of each lysate were diluted to a final volume of 5 ml in the hybridization reaction buffer (final concentrations 500 mM LiCl, 0.5% SDS, 50 mM EDTA, 10 mM Tris, pH 7.5, 14% formamide and Fungal protease inhibitors.) 125 μl of streptavidin Dynabeads (Invitrogen #65002) were washed three times with an equal volume of 1X B&W buffer (5 mM Tris-HCl pH7.5, 0.5 mM EDTA and 1 M NaCl) and once with 0.1 M NaCl. The beads were then incubated with 4 nM of biotinylated oligos complementary to the tag sequence (1.67 nM of each oligo oJC2071, oJC2072 and oJC2073) in 1X B&W buffer at room temperature for 15 min. After immobilization of the biotinylated oligos, beads were washed twice with 1X B&W buffer and incubated with the 5 ml cell lysate at room temperature overnight. Beads were then washed twice with Wash buffer 1 (10 mM Tris-HCl pH7.5, 1mM EDTA, 250 mM LiCl and 0.1% SDS) and three times with Wash buffer 2 (10 mM Tris-HCl pH7.5, 1mM EDTA, 100 mM LiCl). RNA was eluted by adding 93.5 μl DEPC water and heating at 70°C for 2 min. RNA and protein were precipitated and analyzed by Northern and western Blot, respectively. Specifically, RNA was precipitated at −20°C overnight by 0.3 M NaOAc, 1 μl of glycogen (ThermoFisher AM9515) and 95% EtOH, then resuspended with 500 μl LET/SDS (1% SDS in LET buffer). Crosslinking was reversed at 70°C for 15 min and RNA was extracted once with phenol/chloroform/LET followed by another round of heating at 70°C and RNA extraction. RNA was precipitated in 0.3 M NaOAc, 1 μl of glycogen and 95% EtOH at −20°C overnight, then resuspended in 15 μl DEPC water. For protein precipitation, eluate was concentrated in SpeedVac on high heat (37°C) to 1/5 of the original volume and precipitated with 10% TCA at −20°C overnight. Proteins were pelleted at 14,000 rpm for 10 min at 4°C followed by one wash with 80% Acetone. Pellets were air-dried and resuspended in 1X SDS Sample buffer. Crosslink was reversed by heating proteins at 70°C for 1 hr and proteins were denatured at 95°C immediately. For Figures 3A–3C, 2 l of liquid culture (10 mRNA pull-down reactions) were used for each experimental group. 1/10 of sample was used for Northern RNA analysis and 9/10 of sample was used for western protein analysis.

Tandem Affinity Purification

Dhh1p-TAP and associated complexes were purified from yeast cells by TAP method as described in (Rigaut et al., 1999). Briefly, cells (grown to OD_{600} = 1.2-1.3) were pelleted for 5 min, then washed and resuspended in one volume of ice cold buffer (10 mM K-HEPES pH7.9, 10 mM KCl, 1.5 mM $MgCl_2$, O.5 mM DTT, protease inhibitors). The cells were then passed 3 times through a French-press (1,000 to 1,200 psi) and the lysate was centrifuged at 16,500 rpm for 20 min at 4°C. The supernatant was diluted in a final concentration of 10 mM Tris-HCl pH 8.0, 150 mM NaCl, 0.1% NP-40 (IPPI50 Buffer), 50 mg/ml heparin, and incubated with Sepharose 6B beads for 30 min at 4°C then IgG Sepharose 6 Flow for 3 hr at 4°C.The suspension was passed through a Bio-Rad Poly-Prep chromatography column then the beads were washed with 30 ml of IPPI50 Buffer and 10 ml of TEV C Buffer (-EDTA) (10 mM Tris-HCl pH 8.0, 150 mM NaCl, 0.1% NP-40, 1 mM DTT). They were resuspended in 1 ml of TEV C Buffer

(-EDTA) and incubated with 120 units of TEV (tobacco etch virus protease) overnight at 4°C. The eluate was drained into a new column and washed with TEC C-buffer. The TEV supernatant was incubated for 1 hr with calmodulin Sepharose at 4°C in IPPI50 CBB Buffer (10 mM Tris-HCl pH 8.0, 150 mM NaCl, 1 mM $Mg(Ac)_2$, 1 mM imidazole, 2 mM $CaCl_2$, 0.1% NP-40, 10 mM β-mercaptoethanol). After 3 washes with IPPI50 CBB Buffer, the complexes were eluted from the beads using 0.5 ml IPPI50 CEB Buffer (10 mM Tris-HCl pH 8.0, 150 mM NaCl, 1 mM $Mg(Ac)_2$, 1 mM imidazole, 20 mM EGTA, 0.1% NP-40, 10 mM β-mercaptoethanol), 6 times. Proteins were precipitated with 20% TCA on ice for 30 min, pelleted for 30 min at 4°C, washed with acetone-0.05 N HCl, then resuspended in SDS sample Buffer to run on SDS-PAGE. Gels were stained with Coomassie blue. The proteins were identified by mass spectrometry. For RNA analysis, eluates were precipitated in ethanol at −20°C overnight, then RNA was extracted with phenol/chloroform and analyzed by Northern blot.

Northern Blots of Constructs across Sucrose Gradients

Samples were grown in CSM-Leu-Ura and 2% Galactose/Raffinose until mid-log phase. Cells were then vacuum filtered and lysed with frozen 1x lysis buffer (10 mM Tris pH 7.4, 100 mM NaCl, 30 mM $MgCl_2$, 0.5 mg/mL heparin, 1 (OD_{600} = 0.45-0.5). mM DTT, 100 μg/mL cycloheximide, 1% Triton X-100) in a Spex 6870 freezer mill.

For Figure 6E, 20 OD_{260} units were loaded on a 10%–50% (w/w) sucrose gradient prepared using a BioComp Gradient Master (1:48, 81.5°, 17 rpm) in 1x gradient buffer (20 mM Tris pH8, 150 M KCl, 5 mM $MgCl_2$,0.5 mM DTT 100 μg/ml CHX) and spun in a SW 41 Ti rotor for 40000 rpm at 4°C for 3 hr. Gradients were fractionated using a Teledyne Isco Foxy R2 and RNA was extracted using two rounds phenol:chloroform:isoamyl alcohol extraction (1x fraction volume) and isopropanol precipitation (500 μl 300 mM NaOAc pH5.2, 500 μl isopropanol). RNA pellets were isolated by centrifugation at 14,000 rpm at 4°C for 30 min, were washed using 70% ethanol, and the RNA was pelleted once again. Samples were dried, resuspended in 20 μl 1x TE buffer (10 mM Tris pH8, 1 mM EDTA). 20 μl of loading buffer (0.95 ml formamide, 10 μl EDTA, 40 μl H_2O, 0.025% (w/v) Bromophenol blue, 0.025% (w/v) xylene cyanol) was added to each sample. 10 μl of sample from OPT OST4 gradients and 30 μl of sample from non-OPT OST4 gradients were loaded on 1% formaldehyde-agarose gels. The gels were transferred onto Hybond-N+ nylon membranes using the Bio-Rad 785 vacuum blotter. The membrane was probed with ^{32}P end-labeled oligonucleotides antisense to the 3′ UTR prior to the BoxB stem loops (AR-N-16). Blots were imaged using the Typhoon FLA 9500 and quantified in ImageJ.

Preparation of Footprint and RNA-Seq Libraries

Footprints were prepared largely according to existing methods (Guydosh and Green, 2014). Upon vacuum filtration, the cells were frozen in liquid nitrogen and ground in a Spex 6870 freezer mill along with frozen lysis buffer beads (20 mM Tris pH8, 140 mM KCl, 1.5 mM $MgCl_2$, 1% Triton X-100, 100 μg/mL CHX).

For RNA-Seq experiments, ribosomal RNA was subtracted using RiboZero Magnetic Gold (Yeast) from Epicenter, and the remaining RNA was ligated to a universal adaptor. Upon reverse transcription, circularization, and PCR amplification, cDNA fragments were sequenced on either an Illumina HiSeq2000 or HiSeq2500 machine at facilities at UC Riverside or the Johns Hopkins Institute of Genetic Medicine.

For footprint libraries, the above steps were preceded by RNase treatment, 15 U of RNase I (Ambion) per OD_{260} unit of the lysate, and monosome species were separated by sucrose gradient - 10%–50% (w/w) sucrose gradient, prepared as outlined in the section 'Northern blots of constructs across sucrose gradients.' The extracted RNA was purified from a 15% denaturing PAGE gels between markers of the following sizes: 25-34 nt (Original Samples), 15-35 nt (Replicates), with empty lanes left between all samples to prevent cross contamination.

Read Preparation and Sequence Alignment

All gene boundaries and annotations used in analysis are from the R64-1-1 S288C reference genome assembly (sacCer3) from the *Saccharomyces* Genome Database Project. A tab delimited file containing gene annotations was obtained from the UCSC Table Browser (https://genome.ucsc.edu/cgi-bin/hgTables).

De-multiplexed sequences were first processed to remove adaptor sequences (CTGTAGGCACCATCAATAGATCGGAA, Universal miRNA Cloning Linker from NEB) using the CutAdapt tool (Martin, 2011). The remaining reads were then processed to remove low-quality reads (PHRED accuracy < 97.5%).

In addition, contaminating non-coding and ribosomal RNAs were filtered. This was accomplished by alignment to the ncRNA gene database FASTA file available at the *Saccharomyces* Genome Database Project (http://downloads.yeastgenome.org/sequence/S288C_reference/rna/archive/rna_coding_R64-1-1_20110203.fasta.gz). This alignment was performed using Bowtie 1.1.2 (Langmead et al., 2009) using the following parameters: '-Sv 3 –p 4 –best'.

The remaining reads were then aligned to the yeast genome using Bowtie 1.1.2 using he following parameters: ''-Sm 1 –p 4 –best –strata'. Reads were then mapped to the genome to nucleotide resolution using either 3′-end mapping of all read lengths or 5′-end mapping of 28-nt fragments. Once counts are tabulated at each nucleotide position, the values are normalized to reads per million (rpm) which involves dividing counts at each position by the total number of mapped reads. Python and R scripts used to generate the data and figures in this paper can be found on GitHub at https://github.com/greenlabjhmi/2016-Cell-Dhh1.

sTAI of all annotated genes were calculated as per previously outlined methodologies (Sabi and Tuller, 2014). A modification of the previously outlined TAI (tRNA Adaptation Index) metric (dos Reis et al., 2004), this metric does not require fitting to gene expression.

All analysis of mRNA levels and ribosome occupancy looks only at genes that have greater than 128 mapped counts on average across all 18 datasets generated. All genome analysis plots are made using the ggplot2 R package; however, binning by sTAI and %GC content was performed in Python. Only bins of greater than 100 counts were considered to ensure that distributions were well sampled and effects of outliers are minimized. Python analysis scripts and R plotting scripts are also available through GitHub at https://github.com/greenlabjhmi/2016-Cell-Dhh1.

Deep sequencing data for CLIP of Dhh1 (Mitchell et al., 2013) was downloaded from the GEO (Series ID GSE46142).

QUANTIFICATION AND STATISTICAL ANALYSIS

Statistical parameters are reported in the Figures and the Figure Legends. Half-lives of reporter mRNAs were obtained by quantifying the Northern blots signals from biological triplicates. Concerning all genomic-wide analysis, violin plots list the number of genes in each bin as to better represent the distribution of genes across the various metrics (i.e., sTAI, GC content, etc.). Further in these analysis, replicates (where available) were pooled and change in the median of two distributions (e.g., low sTAI/high sTAI) was calculated using a two-tailed Mann-Whitney test, where statistical significance is denoted by a p value less than 0.05. Northern blots taken across polysomes were performed in triplicate and fold enrichment of mRNA is shown with calculated standard error.

DATA AND SOFTWARE AVAILABILITY

Data Resources

The three scripts used in analysis and generation of figures for deep sequencing data are found on https://github.com/greenlabjhmi/2016-Cell-Dhh1. "Pipeline.py" is used to process raw FASTQ files and generate WIG files as outlined in the methods previously. "DataGen.py" uses the previously generated WIG files to create the processed data files required to generate the figures in the paper. These figures are then plotted using the R command "Plot.R."

The accession number for the raw data files as well as per nucleotide counts (WIG files) for the ribosome profiling and RNA sequencing analyses reported in this paper is NCBI Gene Expression Omnibus: GSE81269. The accession number for the raw Dhh1p CLIP data reported in this paper is NCBI Gene Expression Omnibus: GSE46142.

Cell

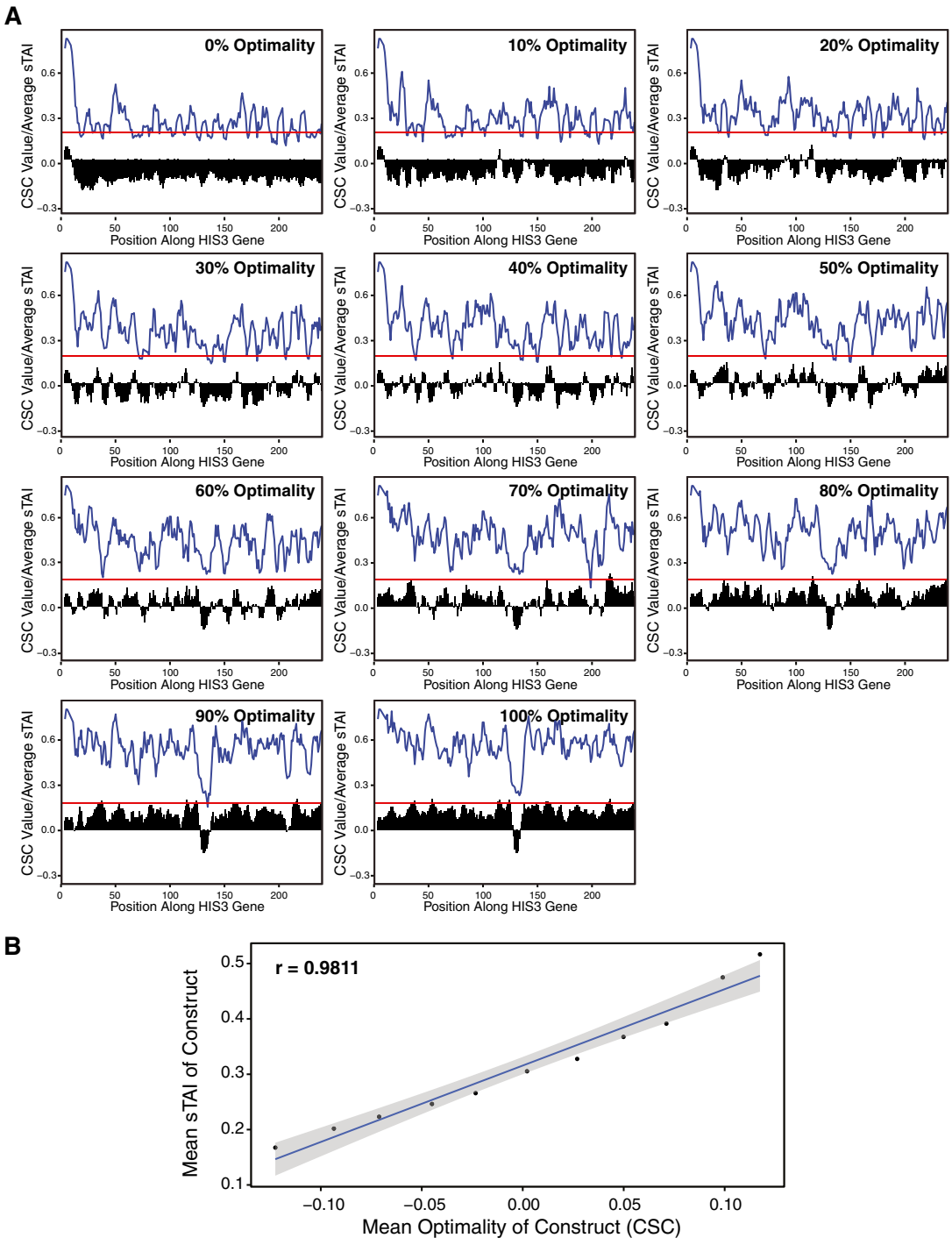

Figure S1. Codon Composition of HIS3 Reporters Varying in Codon Optimality, Related to Figure 1

(A) Graphs for CSC values (black bars) and sTAI values (blue line) averaged across five codon-long windows within the ORF of the *HIS3* reporters. The red line represents the average sTAI across the gene for the 0% optimal *HIS3* reporter. The total percent optimality is shown above each graph. Note the 5′ end of each reporter is tagged with FLAG of consistent codon composition. Moreover, an identical codon stretch is present in all 11 reporters that comprise the probe site used for Northern analysis.

(B) The correlation between the average CSC and average sTAI across the 11 reporters.

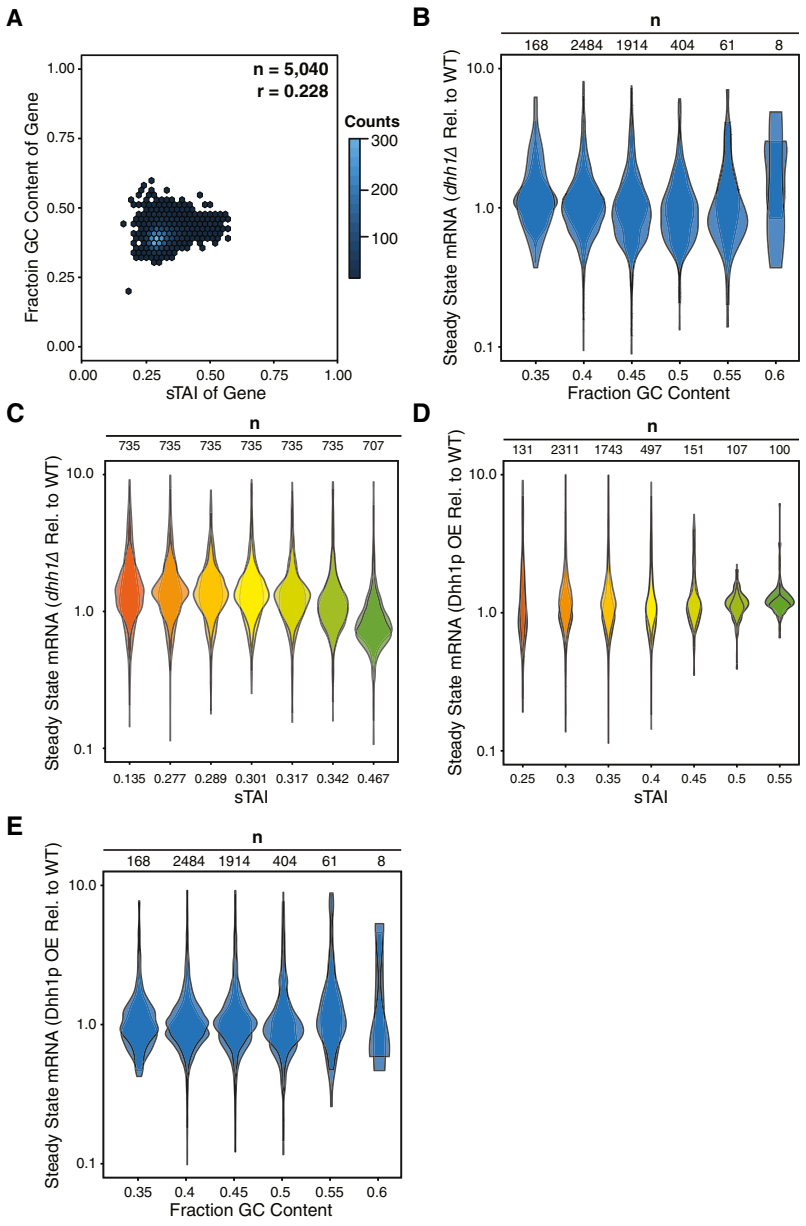

Figure S2. Non-optimality of mRNA Transcripts Is a Proxy for Poor Translation, Related to Figure 2

(A) Species-specific tRNA adaptation index (sTAI) plotted against percent GC content for all protein encoding transcripts in yeast.

(B) Quantifying steady state levels of mRNAs by RNA-Seq in *dhh1Δ* cells (RPKM) relative to WT cells (RPKM) where transcripts are binned by fraction GC content. Shown are two biological replicates. A two-tailed Mann-Whitney test shows that low GC content mRNAs (GC Fraction = 0.3, Med. = 1.33) are not enriched relative to high GC content mRNAs (GC Fraction = 0.55, Med. = 1.36) upon Dhh1p depletion, U = 5210, p = 0.847.

(C) Quantifying steady state levels of mRNAs by RNA-Seq in *dhh1Δ* cells (RPKM) relative to WT cells (RPKM) where transcripts are binned by sTAI where each bin contains an identical number of genes. Shown are two biological replicates. A two-tailed Mann-Whitney test shows that low optimality mRNAs (sTAI = 0.135, Med = 1.41) are enriched relative to high optimality mRNAs (sTAI = 0.467, Med = 0.73) upon Dhh1p depletion, U = 2209, $p < 2.2x10^{-16}$.

(D) Steady state levels of mRNA by RNA-Seq in WT cells where Dhh1p is constitutively overexpressed (OE) relative to WT cells where transcripts are binned by sTAI. Shown are two biological replicates. A two-tailed Mann-Whitney test shows that low optimality mRNAs (sTAI = 0.25, Med. = 1.09) are *not* enriched relative to high optimality mRNAs (sTAI = 0.55, Med. = 1.07) upon Dhh1p overexpression, U = 5412, p = 0.4593.

(E) Steady state levels of mRNA by RNA-Seq in WT cells where Dhh1p is constitutively overexpressed (OE) relative to WT cells where transcripts are binned by fraction GC content. Shown are two biological replicates. A two-tailed Mann-Whitney test shows that low GC content (GC Fraction = 0.3, Med. = 0.95) are *not* enriched relative to high GC content mRNAs (GC Fraction = 0.55, Med. = 1.06) upon Dhh1p overexpression, U = 4102, p = 0.2117.

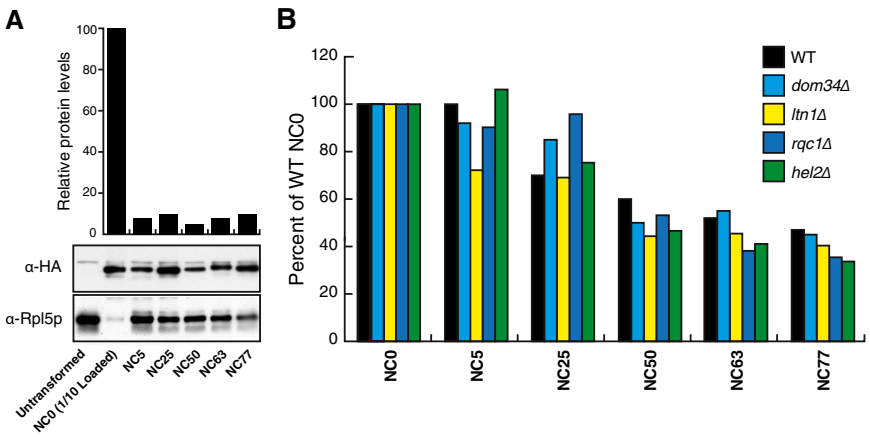

Figure S3. The Polarity of mRNA Degradation Is Dependent on Translation and Ribosome Association with the ORF Upstream of the Non-optimal Stretch, Related to Figures 4 and 5

All experiments in Figure S3 were performed with the *PGK1*-HA reporters containing no stretch (NC0) or a stretch of non-optimal codons (NC) at a given distance from the AUG (5, 25, 50, 63, 77%).

(A) Protein output of the different reporters was analyzed by western blot; relative levels are plotted above. Rpl5p was probed as a loading control.

(B) Relative levels of the *PGK1* reporters in different strains deleted for essential factors involved in the ribosome quality control pathways.

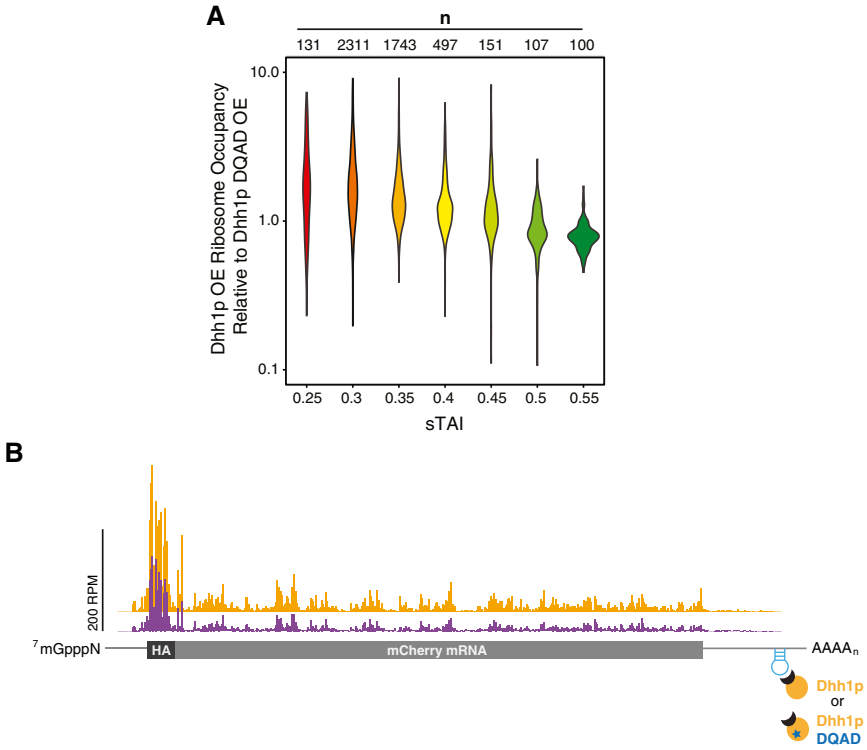

Figure S4. Dhh1p Modulates Ribosome Occupancy on mRNAs with Low Codon Optimality, Related to Figure 6

(A) Plotting the ribosome occupancy (average number of ribosomes per mRNA) for transcripts under constitutive Dhh1p OE relative to constitutive Dhh1p-DQAD OE, binning transcripts by sTAI. Shown are two biological replicates. A two-tailed Mann-Whitney test shows that low optimality mRNAs (sTAI = 0.25, Med. = 1.53) have increased ribosome occupancy relative to high optimality mRNAs (sTAI = 0.55, Med. = 0.71), U = 685, $p < 2.2x10^{-16}$ upon catalytically active Dhh1p overexpression relative to catalytically inactive Dhh1p overexpression.

(B) Ribosome occupancy along a reporter HA-mCherry mRNA upon tethering catalytically active and inactive Dhh1p.